Xue et al. *Zool. Res.* 2026, 47(5): 1453−1470
https://doi.org/10.24272/j.issn.2095-8137.2025.489
https://cstr.cn/32248.14.zr.2025.489

ZR | Zoological Research

Article Open Access

Spexin-GALR2-Gq axis as a biased signaling pathway for colitis therapy

Jing-Wen Xue[1,2,4,#], Ting Zhang[1,2,4,#], Xiang-Lin Kong[3,#], Kun Zheng[1,2,4], Yu-Wei Chen[3], Kai-Li Ma[3], Tao Zeng[1,2,4], Juergen Brosius[1], Fei Xu[5,*], Shan-Shan Lai[3,*], Cheng Deng[1,2,4,*]

[1] *Department of High Altitude Medicine*, *Center for High Altitude Medicine*, *National Clinical Research Center for Geriatrics*, *Frontiers Science Center for Disease-Related Molecular Network*, *West China Hospital*, *Sichuan University*, *Chengdu*, *Sichuan* 610041, *China*

[2] *Institute of High Altitude Medicine*, *High Altitude Medicine Key Laboratory of Sichuan Province*, *West China Hospital*, *Sichuan University*, *Chengdu*, *Sichuan* 610041, *China*

[3] *Jiangsu Key Laboratory for Biodiversity and Biotechnology*, *College of Life Sciences*, *Nanjing Normal University*, *Nanjing*, *Jiangsu* 210023, *China*

[4] *Center for High Altitude Medicine*, *Xining*, *Qinghai* 810000, *China*

[5] *iHuman Institute*, *School of Life Science and Technology*, *ShanghaiTech University*, *Pudong*, *Shanghai* 201210, *China*

ABSTRACT

Inflammatory bowel disease (IBD) remains a major clinical challenge worldwide. Spexin (SPX), a neuropeptide that signals through galanin receptors (GALR2/3), has been implicated in metabolic and behavioral regulation. Here, we report that SPX effectively alleviates colitis, primarily by suppressing inflammation and promoting intestinal epithelial repair, outperforming its relative peptide, galanin (GAL). Mechanistically, SPX exhibits G protein-biased agonism at GALR2, whereas GAL favors β-arrestin2 recruitment. Utilizing *Galr2*$^{-/-}$ and *Galr3*$^{-/-}$ mice, receptor-specific inhibitors, and intestinal epithelial-specific *Gnaq* and *Arrb2* knockout mice, we establish that the SPX-GALR2-Gq axis drives the protective effects of SPX in colitis. Structure-guided mutagenesis further pinpointed key residues governing this signaling bias and enabled the design of SPX p.Lys11Leu, a high-affinity GALR2 agonist that exerts potent anti-colitis activity at significantly lower doses than wild-type SPX. Collectively, our work defines the SPX-GALR2-Gq axis as a therapeutically relevant biased signaling pathway for colitis, and nominates SPX, particularly its p.Lys11Leu mutant, as a promising peptide drug candidate for IBD.

Keywords: Spexin; GALR2; Inflammatory bowel disease; Gq signaling; Biased signaling

INTRODUCTION

Spexin (SPX), also known as neuropeptide Q, is encoded by a 116-amino-acid prepropeptide, which is cleaved into a highly conserved 14-amino-acid mature peptide in mammals (Mills et al., 2021; Tran et al., 2022). The ortholog *SPX1* and paralog *SPX2* genes also yield a 14-amino-acid peptide and have been identified in non-mammalian vertebrates, including fish (Cohen et al., 2020; Zhao et al., 2022), amphibians (Kim et al., 2014), reptiles (Kim et al., 2014), and birds (Meng et al., 2023). Based on sequence and functional similarities, galanin (GAL) and kisspeptin (KISS) are considered part of a common ancestral peptide family with SPX (Kim et al., 2014; Mills et al., 2021). GAL, a 29-amino-acid mature peptide (30-amino-acids in humans due to the lack of amidation at the C-terminus), shares galanin receptors (GALRs) with SPX (Mills et al., 2021). GALRs consist of three members: GALR1, GALR2, and GALR3, all of which are G protein-coupled receptors (GPCRs) (Branchek et al., 2000). GALR1 and GALR3 primarily couple to Gi/o proteins to inhibit the adenylyl cyclase activity and reduce the intracellular levels of 3', 5'-cyclic adenosine monophosphate (cAMP), while GALR2 mainly couples to Gq/11 proteins to stimulate phospholipase C, causing an elevation in cytosolic Ca^{2+} concentrations (Duan et al., 2022; Jiang & Zheng, 2022). While both GAL and SPX

Received: 13 October 2025; Accepted: 02 March 2026; Online: 03 March 2026

Foundation items: National Natural Science Foundation of China (32270438 to C.D., 32170498 to S.L.); National Key R&D Program of China (2021YFF0702000 to C.D.); National Science and Technology Major Project (2023ZD0506800 to C.D.); 1.3.5 project for disciplines of excellence, West China Hospital, Sichuan University (ZYYC21011 to C.D.); National Clinical Research Center for Geriatrics, West China Hospital, Sichuan University (Z2023JC003 to C.D.); Science and Technology Department of Sichuan Province (2022YFH0116 to C.D.); the Priority Academic Program Development of Jiangsu Higher Education Institutions (PAPD to C.D.); the "Kun lun Talents" of Qinghai-Top-Notch and Pioneering talent of Innovation and Entrepreneurship (to C.D.).#Authors contributed equally to this work.

#Authors contributed equally to this work

*Corresponding authors, E-mail: dengcheng2014@126.com; laishanshan@njnu.edu.cn; xufei@shanghaitech.edu.cn

target GALRs, their receptor selectivity profiles diverge: GAL demonstrates high affinity for GALR1/2 and low affinity for GALR3, whereas SPX preferentially binds to GALR2/3 but does not activate GALR1 (Duan et al., 2022; Jiang & Zheng, 2022). Beyond canonical G protein-coupled signaling, GAL can also activate β-arrestin1/2 signaling downstream of GALR2, driving receptor internalization, while SPX exhibits biased agonism toward β-arrestin2 but not β-arrestin1 via GALR2 with lower efficacy than GAL, primarily driving Erk1/2 phosphorylation (Reyes-Alcaraz et al., 2018).

Inflammatory bowel disease (IBD), encompassing Crohn's disease (CD) and ulcerative colitis (UC), is a globally prevalent gastrointestinal disorder, characterized by chronic intestinal inflammation and symptoms including abdominal pain, diarrhea, and weight loss (Massironi et al., 2023). Current therapeutic strategies rely on surgical treatment and pharmacotherapy involving small-molecule drugs, aminosalicylates, corticosteroids, and immunomodulators; however, challenges persist due to side effects, delayed efficacy, drug resistance, and cost limitations (Rogler et al., 2021). This underscores the need for novel therapeutic targets. SPX is widely expressed in the central nervous system including the hypothalamus and hippocampus (Fang et al., 2024; Mills et al., 2021) and peripheral tissues such as the gastrointestinal tract, pancreas, liver, and kidney (Lv et al., 2019; Mills et al., 2021). SPX has been implicated in regulating appetite and body weight (Meng et al., 2023; Zhao et al., 2022), glucose homeostasis and energy metabolism (Fang et al., 2022; Yu et al., 2022), anxiety relief (Reyes-Alcaraz et al., 2016), and reproductive function (Chen et al., 2024). Emerging evidence highlights the regulatory roles of GAL and GALRs in intestinal pathophysiology. Specifically, GALR1 was upregulated in dextran sulfate sodium (DSS)-induced colitis in mice to regulate colonic fluid secretion (Marrero et al., 2000). Immunohistochemical (IHC) staining of colonic biopsies from IBD patients demonstrated the expression of GALR2 and GALR3 within granulocytes (Brunner et al., 2021), and *Galr3*$^{-/-}$ mice exhibited more severe intestinal inflammation and histological damage in DSS-induced colitis compared to wild-type (WT) mice (Brunner et al., 2021). In rats with 2,4,6-trinitrobenzenesulfonic acid (TNBS)-induced colitis, intraperitoneal (i.p.) administration of GAL dose-dependently ameliorated colitis (Talero et al., 2006). GAL can also inhibit gastrointestinal motility and the release of hormones after feeding, such as glucagon, insulin, neurotensin, and somatostatin (Bauer et al., 1989). Research on the role of SPX in intestinal diseases is still limited. SPX is expressed in normal human small intestine and colon tissues, particularly in endocrine and epithelial cells (Gu et al., 2015). In patients with functional constipation, serum SPX levels are significantly reduced (Lin et al., 2015), and SPX can act on GALR2 to modulate bowel motility by activating the L-type voltage-dependent Ca^{2+} channel (VDCC) (Lin et al., 2015). These findings suggest that SPX may also play an important role in colitis; however, the underlying mechanism and therapeutic targets remain unclear.

Here, we traced the evolution of *SPX* and compared the ability of SPX1 and SPX2 to activate GALR2 and GALR3. Intraperitoneal administration of SPX (mammalian SPX1 and non-mammalian chicken SPX2) effectively ameliorated symptoms in DSS- and TNBS-induced colitis mouse models, including reduced weight loss, decreased inflammation, and restoration of colon length, with therapeutic efficacy significantly superior to that of GAL. Mechanistically, SPX alleviated colitis by preferentially activating the GALR2-Gq signaling pathway, rather than the β-arrestin2 pathway. Furthermore, in our investigation of key residues governing the bias of SPX, we discovered the SPX p.Lys11Leu (SPX1^{K11L}) mutant which exhibited enhanced affinity for GALR2 and remarkable therapeutic efficacy for colitis at lower concentrations. Our research not only elucidates the new physiological functions of SPX but also provides insights into the design of Gq-biased GALR2 agonists, thereby opening a potential therapeutic avenue for colitis.

MATERIALS AND METHODS

Animals

The wild-type (C57BL/6JGpt), *GALR2*$^{+/-}$ (C57BL/6JGpt-*Galr2*^{em12Cd7286}, T052656), *GALR3*$^{+/-}$ (C57BL/6JGpt-*Galr3*^{em15Cd3053}, T029757) and *Gnaq*$^{fl/+}$ (C57BL/6JGpt-*Gnaq*^{em1Cflox}, T014948) mouse lines were purchased from GemPharmatech Co., Ltd (China). The *Arrb2*$^{fl/+}$ (C57BL/6Smoc-*Arrb2*$^{em1(flox)}$, 2101681) mouse line was purchased from Shanghai Model Organisms Center, Inc (China). Homozygous lines were generated by heterozygous crosses, with WT littermates as controls. Mice were housed under standard conditions (22±2°C, 50%±10% humidity, 12-hour light/dark cycle) with free access to food and water. All animal experimental procedures complied with the Animal Management Regulations of the Ministry of Health, China (Document No. 55, 2001) and were approved by the Science and Technology Department of Jiangsu Province [Approval No. SYXK (SU) 2020-0047].

Reagents

All peptides (sequences in Supplementary Table S1) were synthesized by Biotech Bioengineering (China) without C-terminal amidation (Lim et al., 2019). Peptide powders were dissolved in sterile water (1 mmol/L stock), aliquoted, and stored at –80°C. The GALR2 antagonist M871 (HY-P1130) and the GALR3 antagonist SNAP37889 (HT-2157) were purchased from MedChemExpress (China), dissolved per the manufacturer's instructions, aliquoted, and refrigerated.

DSS-induced colitis model

Male mice (8–10 weeks old, 25±2 g) were randomly divided into groups. On day 0, the control group received normal drinking water, and the other groups received 3% (w/v) dextran sodium sulfate (36 000–50 000 M.Wt., MP Biomedicals, USA) dissolved in water for 7 consecutive days. Concurrently, the peptide-treatment groups received daily i.p. injections of 100 μL of 3 μmol/L peptide solution, and the control and DSS groups received the same volume of saline. In experiments involving inhibitor treatment, mice received an i.p. injection of 100 μL of antagonist solution (10 nmol) 30 min prior to SPX peptide. Body weight and disease activity index (DAI) scores (criteria in Supplementary Table S2) were assessed daily. On day 7, mice were euthanized after undergoing colonoscopy. The entire colon was then harvested, measured for length, and photographed. Colon tissue samples were collected from the same region for total RNA extraction and histological analysis.

TNBS-induced colitis model

The 5% (w/v) 2,4,6-trinitrobenzenesulfonic acid (Sigma-Aldrich, USA) stock solution was diluted to 2.5% (w/v) with

anhydrous ethanol. Male mice (8–10 weeks old) were randomly assigned to groups. On day 0, mice were anesthetized and given an enema following established guidelines (Wirtz et al., 2017; Zheng et al., 2017), then administered 100 μL of 2.5% TNBS or 50% ethanol (control) intrarectally using a flexible catheter inserted approximately 4 cm. Mice were monitored until fully recovered from anesthesia and then returned to their cages for normal feeding. Peptide-treated mice received daily i.p. injections of 100 μL of 3 μmol/L peptide solution, and the other groups received the same volume of sterile saline. Body weight was recorded daily for all mice. On day 3, mice underwent colonoscopy and were subsequently euthanized. The entire colon was excised, and its length was measured and photographed. Colon tissue samples were collected from a consistent region for subsequent analyses.

ELISA

Serum was isolated from whole blood collected from mice, and serum SPX levels were quantified using commercially available ELISA kits (SPX, YJ251105; IL-1B, YJ301814; IL-6, YJ098430; TNFA, YJ002095) purchased from YuanjuBio (China), according to the manufacturer's instructions.

RNA isolation and RT-qPCR

Colon tissues for RNA extraction were immediately snap-frozen in liquid nitrogen and stored at –80°C. Total RNA was isolated using TRIzol reagent (Vazyme, R711-01, China), adhering to the manufacturer's guidelines. RNA quality and quantity were then assessed via capillary electrophoresis (NanoDrop 2000, Thermo Fisher Scientific, China). One μg of RNA was reverse transcribed into cDNA using a PrimeScript RT reagent kit with gDNA Eraser (Vazyme, R323-01, China). Target gene expression was quantified by real-time PCR using SYBR Green (Vazyme, Q312, China) in a LightCycler 96 PCR system (Roche, Switzerland). Primer sequences, obtained from Tsingke Biotech Co., Ltd (China), are detailed in Supplementary Table S3. Relative gene expression levels were normalized to *Actb* using the $2^{-\Delta Ct}$ method.

RNA-sequencing and analysis

Raw sequencing reads of mouse colon tissues were generated using the Illumina Novaseq 6000 platform by Novogene Co., Ltd (China). Following quality control, clean reads were aligned to the *Mus musculus* reference genome using HISAT2. Gene expression quantification was performed by calculating read counts mapped to each gene using featureCounts, and then normalized to Transcripts Per Million (TPM) to account for sequencing depth and gene length. Datasets from GSE59071 (healthy=11; presence of ulcers, CD active=8; endoscopic Mayo subscore 0–1, UC inactive=23; endoscopic Mayo subscore 2–3, UC active=74) (Vanhove et al., 2015), GSE9452 (healthy=5; with no macroscopic signs of inflammation, UC uninflamed=13; with macroscopic inflammation, UC inflamed=8) (Olsen et al., 2009), and GSE16879 (healthy=6, CD=37, UC=48) (Arijs et al., 2009) were downloaded from the Gene Expression Omnibus (GEO) database. The RNA-seq data from E-MTAB-9850 (mice were treated with 3% DSS for 8 days; day 0, healthy=3; day 3, inflamed-medium=2; day 8, inflamed-high=3; day 12, recovery-moderate=3; day 19, recovery-full=3) (Gonzalez Acera et al., 2021) were obtained from ArrayExpress. Box plots display the median (horizontal line), the 25th and 75th percentiles (box limits), whiskers representing 1.5 times the interquartile range (IQR), with individual data points depicted as jittered dots. Expression data for *hsGALR2*, *hsGALR3*, and *SPX* in intestinal cells were obtained from the Human Protein Atlas. Analysis of differentially expressed genes (DEGs) was performed using DESeq2 in R. Genes with an absolute $\log_2$(fold change)≥1 and an adjusted *P*-value<0.05 were considered significantly differentially expressed. Significantly enriched Gene Ontology Biological Processes (GO-BP) and Kyoto Encyclopedia of Genes and Genomes (KEGG) pathways were identified using the clusterProfiler package in R, employing a *P*-value cutoff of 0.05. Gene Set Variation Analysis (GSVA) was performed using the GSVA package in R to estimate the relative enrichment of specific gene sets in each sample. We utilized the mMCP-counter package in R to estimate the abundance of tissue-infiltrating immune, epithelial, and endothelial cell populations in mouse samples.

Histological staining and scoring

Colon tissues from mice were fixed in 4% paraformaldehyde (Biosharp, BL539A, China), processed for paraffin embedding, sectioned, and then stained with hematoxylin and eosin (H&E) for histological analysis. Microscopic evaluation of the H&E-stained sections focused on assessing inflammatory cell infiltration (scored 0–3 based on severity and depth), crypt architecture (scored 0–4 reflecting the extent of architectural distortion and loss), and lesion extent (scored 0–3 according to the distribution of the pathology), with the final score for each sample representing the sum of these three subscores (Zhou et al., 2023).

Immunohistochemical staining

Intestinal sections were deparaffinized, rehydrated, and subjected to heat-induced epitope retrieval. Endogenous peroxidase activity was quenched with hydrogen peroxide, and non-specific antibody binding was blocked. Sections were then incubated overnight at 4°C with primary antibodies against TJP1 (Proteintech, 21773-1-AP, China; 1:3 000) and OCLN (Proteintech, 13409-1-AP, China; 1:200). Immunoreactivity was visualized using HRP-conjugated secondary antibodies and a DAB substrate kit (CST, 8059S, USA). Finally, sections were counterstained with hematoxylin to facilitate microscopic examination.

Western blotting

Total protein was extracted from colon tissues using RIPA lysis buffer (Epizyme, PC101, China) supplemented with protease inhibitors (Epizyme, PC101, China) and phosphatase inhibitors (Epizyme, PC102, China). Protein concentrations were determined by a BCA assay kit (Epizyme, ZJ101, China). Equal amounts of protein (30 μg per lane) were separated by 10% SDS-PAGE (Epizyme, LK404, China) and transferred onto PVDF membranes. After blocking with a blocking buffer (Epizyme, PS108P, China) for 1 h at room temperature, the membranes were incubated overnight at 4°C with primary antibodies against TJP1 (Proteintech, 21773-1-AP, China; 1:2 000), OCLN (Proteintech, 13409-1-AP, China; 1:2 000) or ACTB (Abways, AB2001, USA; 1:5 000). Following extensive washing, the membranes were incubated with HRP-conjugated secondary antibodies (Abways, AB0101, China; 1:5 000) for 1 h at room temperature. Protein bands were visualized using enhanced chemiluminescence (ECL) substrate (Vazyme, E422, China) and imaged on a gel imaging system (Shenhuabio, China). After imaging, the membranes were treated with a rapid stripping buffer

(Epizyme, PS107, China) to remove bound antibodies, followed by re-incubation with another primary antibody. Band intensities were quantified with ImageJ software by normalizing target protein signals to ACTB. Statistical comparisons were performed using triplicate biological replicates.

Transmission electron microscopy

Colon tissues were rapidly dissected, opened longitudinally, and rinsed with ice-cold PBS to clear luminal contents, followed by immersion in electron microscopy fixative (Biossci, BP0130, China) at 4°C. For specimen preparation, tissues were rinsed three times (10 min each) in 0.1 mol/L phosphate buffer (PB, pH 7.4), post-fixed with 1% osmium tetroxide in the same buffer for 2 h at room temperature in the dark and then washed again three times (15 min each) with PB. Following dehydration through a graded ethanol and acetone series, samples were infiltrated and embedded in SPI-Pon 812 resin. Ultrathin sections (70 nm) were cut on a Leica UC7 ultramicrotome, collected on 200-mesh copper grids, and stained with uranyl acetate and lead citrate. Imaging was carried out using a Hitachi HT7700 transmission electron microscope. Images were acquired systematically from representative fields for ultrastructural assessment of epithelial morphology.

Plasmids

Galanin receptors were synthesized by General Bio Co., Ltd (China) and subsequently cloned into both pcDNA3.1-V5/His and Tango vectors. Point mutations were introduced using the Mut Express II Fast Mutagenesis Kit V2 (Vazyme, C214, China) according to the manufacturer's protocol and validated by Sanger sequencing. The cAMP response element (CRE), T-lymphocyte activation of nuclear factor-responsive element (NFAT-RE), serum response element (SRE), and serum response factor response element (SRF-RE) luciferase reporter plasmids were obtained from Promega (USA).

Cell culture, transfection and luciferase assay

HEK293 cells and HTLA cells (Kroeze et al., 2015), a HEK293T derivative expressing a tTA-dependent luciferase reporter and β-arrestin2-TEV fusion gene, were cultured in Dulbecco's modified Eagle's medium (DMEM; Gibco), supplemented with 10% fetal bovine serum (FBS, Gibco, USA), 1% penicillin and 1% streptomycin (Gibco, USA). HTLA cells were additionally maintained with puromycin (1 μg/mL, Gibco, USA) and hygromycin (100 μg/mL, Gibco, USA). All cells were incubated at 37°C under a 5% CO_2 atmosphere. For transfection, 96-well plates were coated with poly-L-Lysine, followed by washing with PBS. HEK293 or HTLA cells were seeded into the prepared 96-well plates. Transfection was performed using Lipofectamine-6000 (Beyotime, China) according to the manufacturer's instructions, with 50 ng of receptor plasmid and 30 ng of reporter plasmid per well. After 12 h, the medium was replaced with fresh, complete culture medium. At 36 h post-transfection, peptide stock solutions were diluted to various concentrations using serum-free Opti-MEM medium (Gibco, USA). The old medium was removed, and the cells were incubated with the diluted peptides for an additional 6 h. Luciferase activity was measured using the Luciferase Reporter Gene Assay Kit (Yeasen, China). Luminescence was detected immediately after substrate addition using an EnVision™ Multilabel Plate Reader (PerkinElmer, USA) and then normalized as fold changes relative to control. All experiments were performed in at least triplicate.

Signaling bias analysis

The ΔΔlogRAi parameter was used to analyze signaling bias, revealing differences in both the efficacy and potency of the two pathways, as shown in the following equation (Zhao et al., 2023).

$$\Delta\Delta\text{logRAi}=\log_{10}\left(\left[\frac{E_{max,p1}EC_{50,P2}}{EC_{50,P1}E_{max,p2}}\right]_{ligand}\left[\frac{E_{max,p2}EC_{50,P1}}{EC_{50,P2}E_{max,p1}}\right]_{reference}\right)$$

We calculated the ΔΔlogRAi parameter for ggGAL, SPX1, and ggSPX2, using hsGAL as the reference ligand. Emax and EC_{50} values for each ligand were derived from dose-response curves generated using GraphPad Prism. Data were obtained from distinct pathways: G protein signaling assessed via CRE-Luc, NFAT-Luc, SRE-Luc, and SRF-Luc reporter assays (P1), and β-arrestin2 recruitment measured using the Tango assay (P2). ΔΔlogRAi>0 indicates a bias towards G protein signaling, while ΔΔlogRAi<0 indicates a bias towards β-arrestin2 signaling.

AAV delivery

Adeno-associated virus (AAV) serotype 2/8 (AAV*2/8*) with a villin (Vil) promoter was used to target epithelial cell infection (Arpin et al., 1988; El Marjou et al., 2004; Polyak et al., 2012). The Vil-MCS-3FLAG-2A-EGFP-bGH PolyA vector served as the backbone for constructing AAV viruses. The control virus, designated AAV8-Vil-null, consisted of the vector alone. The experimental virus, AAV8-Vil-Cre, was generated by cloning the *Cre* recombinase gene into the multiple cloning site (MCS). All viruses were ordered from Genechem Co., Ltd (China). Eight- to ten-week-old *Gnaq*$^{fl/fl}$ and *Arrb2*$^{fl/fl}$ mice were randomly assigned to groups and subjected to AAV administration via enema, following the same procedure as described for TNBS treatment. Each mouse received 100 μL of virus solution, with a total dose of 1×10^{11} v.g. To obtain *Gnaq*$^{\triangle Vil}$ or *Arrb2*$^{\triangle Vil}$ conditional knockouts, mice were administered AAV8-Vil-Cre, while control mice received AAV8-Vil-null. One week following AAV administration, colitis was induced by administering 2% DSS in drinking water.

Selection analysis

Full-length protein coding nucleotide sequences of target genes were retrieved from the NCBI database and translated into protein sequences using MEGA v.10.0 (Kumar et al., 2018). Following alignment, the sequences were back-translated to nucleotides, and gap regions were removed. A Neighbor-Joining (NJ) tree was constructed with 1 000 bootstrap replicates. Selection pressure was then estimated using the EasyCodeML v.1.4 (Gao et al., 2019) visualization program with preset mode. Different models were tested. Models with a likelihood ratio test (LRT) *P*-value<0.05 were considered significant. Sites with Bayes Empirical Bayes (BEB) posterior probabilities>0.95 were annotated with asterisks (*), indicating strong evidence of positive selection.

Bioluminescence resonance energy transfer 2 (BRET2) assay

To investigate the dissociation of Gαq-βγ heterotrimer, we employed the Bioluminescence resonance energy transfer 2 (BRET2) assay as previously described (Olsen et al., 2020). Briefly, HEK293T cells were seeded in 10-cm dishes and cultured for 20 h. Cells were then transfected using

Lipofectamine 2000 (Thermo Fisher Scientific, USA) with receptor, Gαq-RLuc8, Gβ, and Gγ-GFP2 constructs (1 μg each, 1:1:1:1 ratio). 24 h post-transfection, cells were harvested and seeded into poly-L-lysine coated 96-well plates (white clear bottom) at a density of 30 000–50 000 cells/well. The next day, white backings were applied to the plate bottoms, and the culture medium was removed. Cells were equilibrated with 40 μL of Hank's Balanced Salt Solution (HBSS) for 5 min at room temperature and then incubated with 40 μL of the test peptide solution at various concentrations for 5 min. Luminescence measurements were initiated by adding 20 μL of coelenterazine 400a (25 μmol/L final concentration; Yeasen, China) using an LB943 Mithras plate reader (Berthold Technologies, Germany) with 410 nm (RLuc8) and 515 nm (GFP2) emission filters, at integration times of 1 second per well. BRET2 ratios were calculated as GFP2/RLuc8 emission values and normalized to vehicle controls. Concentration-response curves were generated in GraphPad Prism v.9.0 through nonlinear regression analysis using a four-parameter logistic (4PL) sigmoidal model, with X-axis values representing log-transformed compound concentrations.

β-arrestin complementation assay

To enable detection of β-arrestin2 recruitment, NanoLuc was split into two complementary fragments: an N-terminal fragment (N1) comprising amino acids 1–102, and a C-terminal fragment (N2) comprising amino acids 103–172 (Hauge Pedersen et al., 2021). Two fusion constructs were generated: mem-linker-N1 (membrane tethered N-terminal split, MeN) and N2-linker-β-arrestin2 (β-arrestin2 tethered C-terminal split, ArC2). HEK293 cells were seeded onto poly-L-lysine coated 96-well plates (white, clear bottom) at a density of 3.5×10^5 cells/mL. After 24 h, cells were transfected with receptor, MeN, and ArC2 constructs at a ratio of 2:1:1. Following a 24-hour incubation period post-transfection, cells were washed twice with D-PBS and then incubated with 80 μL/well of BRET buffer at 37°C for 30 min. During this incubation, peptide ligands and the coelenterazine substrate were prepared at a working concentration of 5 μmol/L. After incubation, the plate was transferred to a microplate reader, and 10 μL/well of coelenterazine was added. The plate was equilibrated at 28°C for 5 min, and luminescence readings at 460 nm were recorded every minute. Subsequently, 10 μL/well of ligand was added, and luminescence readings were continued for an additional 30 min. Dose-response curves were generated to assess the extent of β-arrestin2 recruitment in GraphPad Prism by removing baseline and column math and calculating the area under the curve (AUC).

Structural visualization

Molecular graphics and visualization were performed using PyMOL. The Cryo-EM structure of the SPX1-hsGALR2-Gnaq complex (PDB: 7XJL) was imported into PyMOL for structural analysis. For residue-specific mutagenesis, the Mutagenesis Wizard tool was employed to select target amino acid residues, followed by rotamer optimization using default parameters (energy minimization cutoff: 0.5 Å, maximum clashes: 3). All visual representations were prepared using a combination of cartoon diagrams and surface rendering, with key interacting residues highlighted in stick representation.

Statistical analysis

Data were presented as mean±SEM. Statistical comparisons were performed using Student's *t*-tests for two-group comparisons, one-way analysis of variance (ANOVA) for three or more comparisons, and two-way repeated measures ANOVA for repeated measures data. The number of animals per group in mouse model experiments is described in each figure legend. For dose-response experiments, data were normalized as fold changes relative to control and fitted to a three-parameter log(agonist) vs. response curve using nonlinear regression analysis. All experiments were performed with at least three biological replicates. Statistical analyses were conducted using GraphPad Prism v.9.0 and statistical significance was determined when $P<0.05$.

RESULTS

Phylogenetic divergence of *SPX* across vertebrates

To elucidate the evolutionary trajectory of *SPX*, we first reconstructed its phylogenetic origins (Figure 1A; Supplementary Figure S1), given its hypothesized shared ancestry with *GAL* and *KISS* peptide genes (Kim et al., 2014; Mills et al., 2021). While the ancestral *GAL* and *KISS2* genes were present in the sea lamprey, *SPX* was notably absent. *SPX* emerged later in the vertebrate lineage, with its earliest identifiable homologs localized to cartilaginous fishes (Supplementary Table S4), where it underwent gene duplication and divergence, giving rise to *SPX1* and *SPX2*. Subsequent lineage-specific copy number variations, likely driven by whole-genome duplication events (Berthelot et al., 2014), resulted in paralog diversification (*SPX1a/1b* and *SPX2a/2b*) across teleosts and amphibians. The loss of *SPX2* occurred within the mammalian lineage, with monotremes such as *Tachyglossus aculeatus* exhibiting a complete absence of both *SPX1* and *SPX2* (Supplementary Figure S1).

To further delineate the evolutionary trajectory of *SPX*, we specifically investigated the *SPX2* gene in avian species. *SPX2* is predicted to have four exons, with exons 3–4 encoding the mature peptide (Supplementary Figure S2) (Meng et al., 2023). The *SPX2* gene was consistently identified in *Galliformes* species (e.g., *Gallus gallus*, *Meleagris gallopavo*, *Tympanuchus pallidicinctus*, *Lagopus leucura*, *Phasianus colchicus*, and *Numida meleagris*) and *Struthioniformes* (e.g., *Struthio camelus*). Although *SPX2* was not annotated in *Falconiformes* (e.g., *Falco punctatus*), *Accipitriformes* (e.g., *Aquila chrysaetos*), *Gaviiformes* (e.g., *Gavia stellata*), and *Gruiformes* (e.g., *Grus americana*), full-length coding sequences could be identified through targeted genome sequence alignments. Conversely, other avian families exhibited either partial exon loss (e.g., *Cygnus atratus*, *Anas platyrhynchos*, *Lonchura striata*, and *Calidris pugnax*) or complete sequence loss (e.g., *Cuculus canorus* and *Columba livia*). These findings suggest either taxon-specific assembly gaps or divergent evolutionary pressures shaping *SPX2* retention across avian clades. Collectively, the dynamic evolutionary trajectory of *SPX1/2* establishes it as a highly adaptable peptide family, capable of undergoing significant structural and functional diversification across vertebrate lineages.

SPX1/2 peptides exhibit functional conservation

Despite sharing identical cleavage sites, SPX1 and SPX2 mature peptides exhibited divergent evolutionary profiles, with SPX1 being broadly conserved and SPX2 more variable across species (Figure 1B, C). To evaluate functional

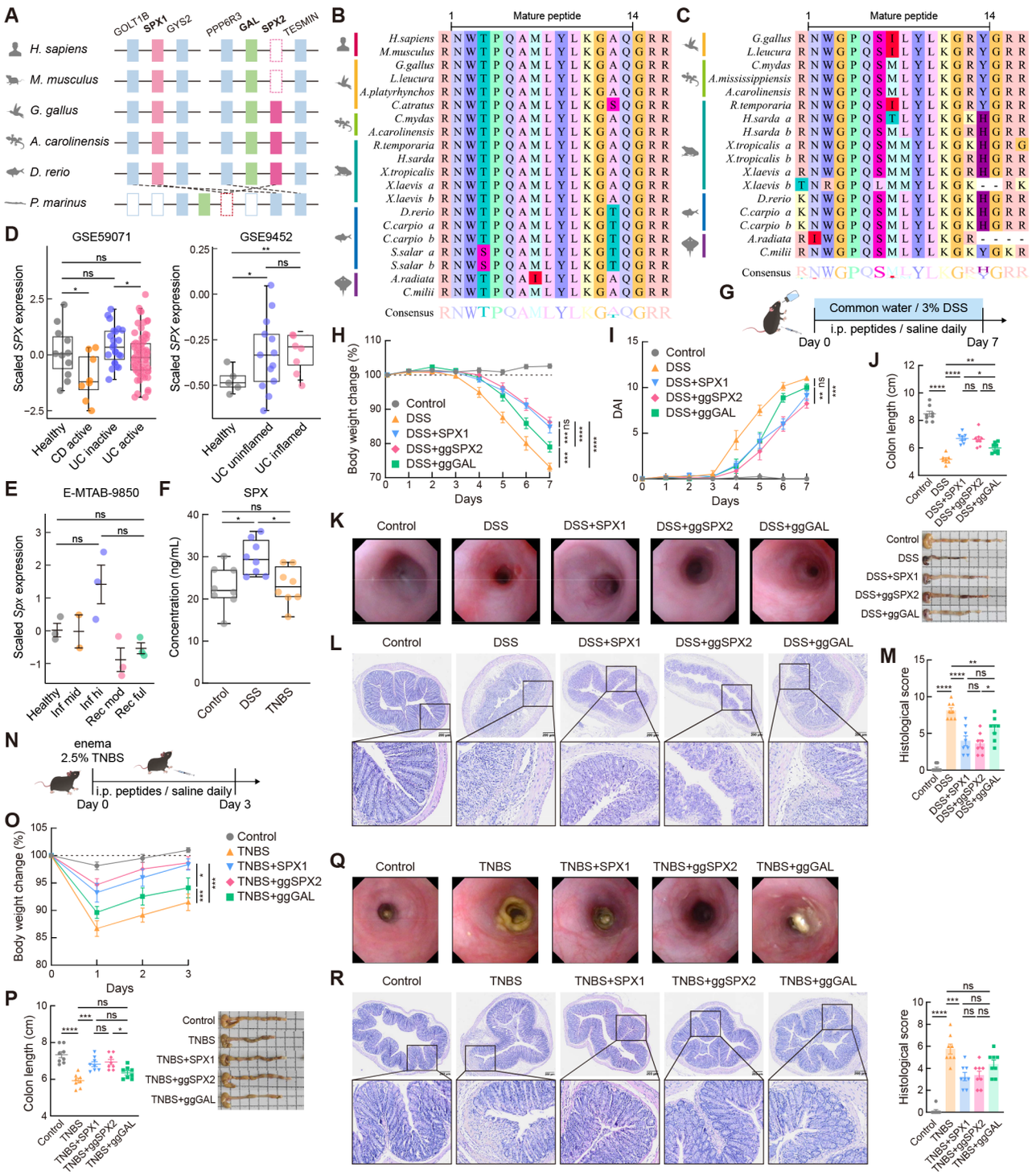

Figure 1 SPX exhibits superior therapeutic efficacy compared to GAL in colitis

A: Gene loci of representative vertebrate *SPX1* and *SPX2*. Dashed boxes indicate gene loss. Solid and unfilled boxes represent presence of other genes at that location. B: Sequence alignment of vertebrate SPX1. C: Sequence alignment of non-mammalian SPX2. D: *SPX* expression in colon tissues from healthy individuals and IBD patients. Data from GSE59071 (left) and GSE9452 (right). E: Dynamic *Spx* expression in DSS-induced colitis mice. Data from E-MTAB-9850. Detailed grouping information is provided in the Methods section. F: Serum SPX levels in control, DSS-treated, and TNBS-treated mice measured by ELISA (n=8, each). G–M: 3% DSS-induced colitis mouse model. N–R: TNBS-induced colitis mouse model. G, N: Flowchart of mouse model. Mice were randomly divided into groups (n=8, each): Control (grey), DSS/TNBS (orange), DSS/TNBS+SPX1 (blue), DSS/TNBS+ggSPX2 (pink), and DSS/TNBS+ggGAL (green). Peptide-treated groups received daily i.p. injections of peptide solution. H, O: Daily body weight changes. Statistical significance for day 7/3 is indicated. I: Daily DAI scores. J, P: Colon length and colon images. K, Q: Colonoscopy images. L, R: H&E staining of colon sections. M: Histological scores of H&E-stained colon sections. Data were analyzed using two-sided Student's t test or one-way/two-way ANOVA and presented as mean±SEM. ns: Not significant; *: P<0.05; **: P<0.01; ***: P<0.001; ****: P<0.0001.

conservation, we synthesized representative SPX1/2 peptides (Supplementary Table S1) and profiled their signaling capacities through GALR2/3 receptors using luciferase reporter assays. We selected the highly conserved tetrapod SPX1 (shared by human, mouse, and chicken) along with representative SPX2 peptides from chicken (ggSPX2), green anole (acSPX2), zebrafish (drSPX2), and medaka (olSPX2) (Supplementary Figure S3). These peptides were tested for activation of human (hsGALR2, hsGALR3), mouse (mmGALR2, mmGALR3), and chicken (ggGALR2, ggGALR2b (Ho et al., 2012), ggGALR3) receptors using CRE-Luc (Gs), NFAT-Luc (Gq/11), SRE-Luc (Gi/o), and SRF-Luc (G12/13) reporters in HEK293 cells to partially represent respective G-protein pathways (Azimzadeh et al., 2017; Cheng et al., 2010; Guo et al., 2022; Liu & Wu, 2004; Rodrigues & McLoughlin, 2009). β-arrestin2 recruitment was further evaluated using the PRESTO-Tango system in HTLA cells (Kroeze et al., 2015). Our results showed that despite sequence divergence across species, SPX peptides exhibited cross-species activation of GALR2/3 and triggered conserved downstream signaling pathways (Supplementary Figure S3). Specifically, SPX1/2 potently activated GALR2 orthologs and ggGALR3, while activation of hsGALR3 and mmGALR3 was comparatively weak (Supplementary Figure S3B-F). Moreover, SPX peptides with different sequences exhibited distinct receptor affinities, with SPX1 and ggSPX2 generally displaying higher activation capabilities for human and mouse receptors, which were selected for our subsequent studies. Taken together, SPX demonstrates a conserved ability to activate GALR2/3 across species despite sequence divergence, underscoring its fundamental role in downstream signaling.

SPX shows superior therapeutic efficacy compared to GAL in treating colitis

Given the established role of GAL in treating intestinal diseases (Bauer et al., 1989; Talero et al., 2006), we sought to explore the potential of SPX, commencing with GEO analyses of SPX expression in human subjects. The results revealed decreased *SPX* mRNA expression in CD patients compared to healthy controls but increased or unchanged levels in UC patients (Figure 1D). In DSS-induced colitis mice (a model for UC), *SPX* mRNA was upregulated during the inflammatory phase and returned to baseline during the recovery phase (Figure 1E). To further validate these changes, we established both DSS-induced UC and TNBS-induced CD mouse models. At the end of modeling, serum SPX peptide levels were elevated in DSS-treated mice, while no significant change was observed in TNBS-treated mice (Figure 1F). These findings suggest that SPX expression in IBD varies by disease subtypes and inflammatory phase, indicating possible pathogenic downregulation or compensatory upregulation at certain disease stages, and further mechanistic studies are warranted to elucidate the precise role of SPX in IBD pathogenesis.

Next, we investigated the therapeutic potential of SPX for colitis *in vivo*. To contextualize its efficacy, we also included chicken GAL (ggGAL), which exhibited comparable therapeutic efficacy compared to human GAL (hsGAL) (Lai et al., 2025). In the DSS-induced UC model, mice received daily intraperitoneal injections of SPX1, ggSPX2, or ggGAL (Figure 1G). DSS administration induced significant weight loss, elevated disease activity index (DAI) scores, colon shortening, and rectal bleeding, confirming successful colitis induction (Figure 1H–J). Colonoscopy revealed intestinal ulcerations (Figure 1K), and histological analysis of hematoxylin-eosin staining (H&E) showed extensive inflammatory cell infiltration, mucosal thickening, and disrupted tissue architecture (Figure 1L, M). All three peptide-treatment groups alleviated these pathological features. Notably, both SPX1 and ggSPX2 demonstrated superior therapeutic efficacy compared to ggGAL, with no significant difference observed between SPX1 and ggSPX2 (Figure1H–M). In the TNBS-induced CD model, mice were treated with respective peptides daily for three consecutive days (Figure 1N). Following TNBS challenge, mice exhibited marked weight loss followed by gradual recovery (Figure 1O). Gross examination revealed diarrhea, intestinal bloating, and colon shortening (Figure 1P). Colonoscopic assessment showed mucosal congestion with adherent fecal residue (Figure 1Q), and histology confirmed inflammatory infiltration, mucosal thickening, and architectural disorganization (Figure 1R). Treatment with SPX1 or ggSPX2 again significantly ameliorated these changes and outperformed ggGAL (Figure 1O–R). These results from both colitis models identified SPX as a novel peptide therapeutic for colitis, with superior efficacy compared to the related galanin peptide.

SPX ameliorates inflammation and restores the epithelial barrier in colitis

To elucidate the superior therapeutic efficacy of SPX over GAL in colitis, we performed RNA sequencing (RNA-seq) on colon tissues from DSS-induced colitis mice in control, DSS, DSS+SPX1, DSS+ggSPX2, and DSS+ggGAL groups (Supplementary Figure S4A). DESeq2 analysis revealed 483 and 770 DEGs in DSS+SPX1 and DSS+ggSPX2 groups, respectively, compared with the DSS+ggGAL group, while only 222 DEGs differed between DSS+SPX1 and DSS+ggSPX2 (Figure 2A; Supplementary Figure S4B–D). GO enrichment analysis for BP and KEGG pathway analysis revealed that SPX treatment enhanced immune responses, cell proliferation and differentiation, and cell adhesion pathways, while suppressing chemotaxis, cell migration, and extracellular matrix-related processes (Supplementary Figure S4E–H). GSVA further revealed that SPX exhibited significantly enhanced regulatory effects on immune- and epithelial-related pathways compared to GAL (Figure 2B–E), whereas both SPX1 and ggGAL showed substantial regulatory capacity on endothelial-related pathways (Supplementary Figure S4I, J). This differential regulation suggested that the superior therapeutic efficacy of SPX may stem from its specific modulation of epithelial barrier function. Consistently, differential expression analysis showed that SPX significantly modulated representative genes involved in inflammation (e.g., *Il1b*, *Il6*, *Tnfa*, *Ccl2*, *Stat3*), cell proliferation (e.g., *Mki67*, *Igf1*, *Myc*), intestinal stem cells (ISCs) and epithelial differentiation (e.g., *Lgr5*, *Sox9*, *Atoh1*, *Gata6*), epithelial barrier (e.g., *Tjp1*, *Ocln*, *Muc2*), and endothelial cell adhesion (e.g., *Icam1*, *Vcam1*, *Pecam1*), illustrating the multi-target activity of SPX in mitigating colitis (Figure 2F). Serum ELISA and RT-qPCR validated the transcriptional changes observed in RNA-seq, as SPX treatment robustly suppressed pro-inflammatory cytokines (*Il1b*, *Il6*, *Tnfa*) and upregulated epithelial barrier-associated genes (*Tjp1*, *Ocln*, *Muc2*) (Figure 2G; Supplementary Figure S5A, B), consistent with the expression profile of corresponding genes in TNBS-induced colitis mice (Supplementary Figure S5C, D). Western blot

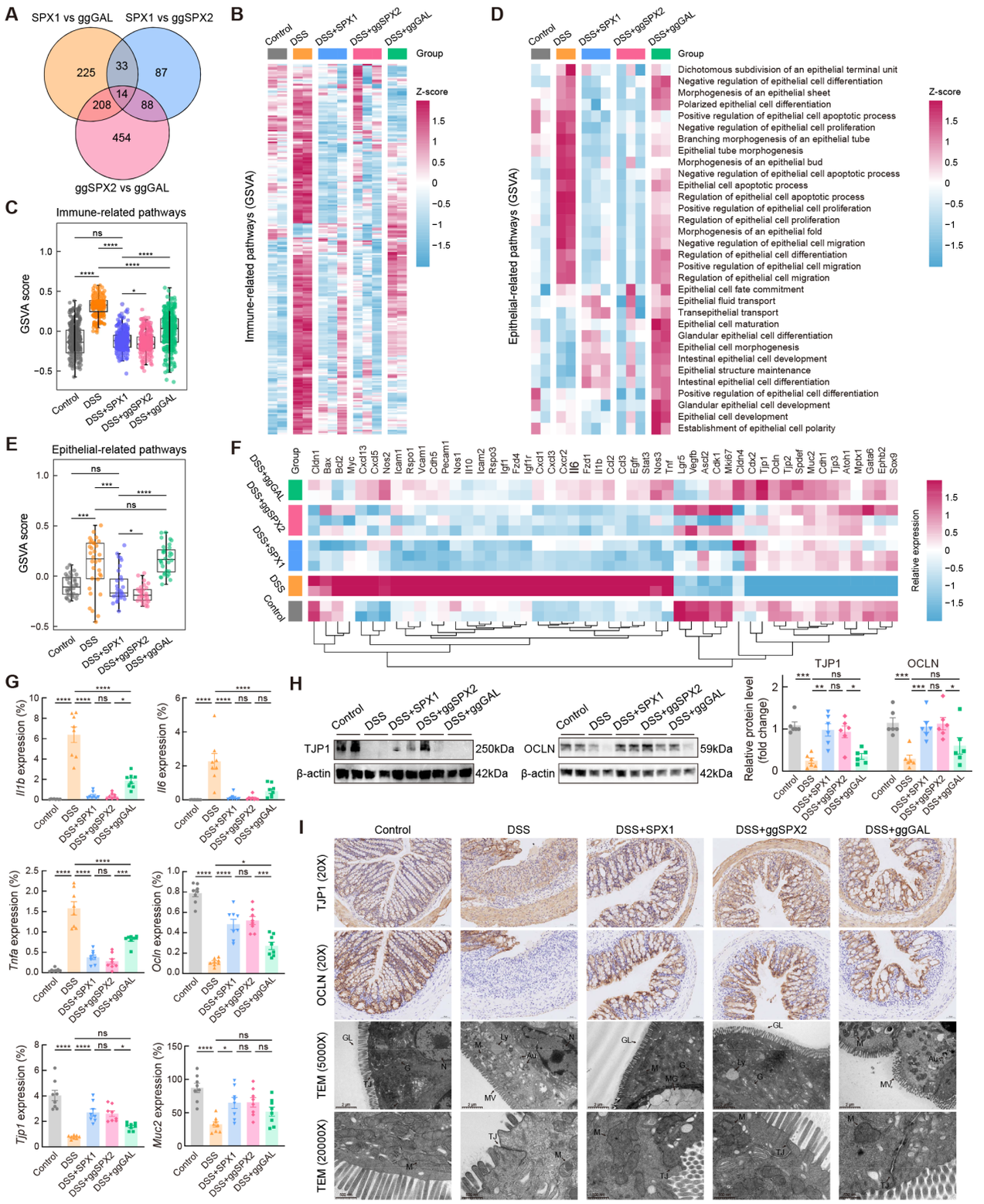

Figure 2 SPX attenuates inflammation and promotes epithelial barrier restoration in colitis, outperforming GAL

RNA-sequencing was performed on colon tissue samples from DSS-induced colitis mice: Control, DSS, and DSS+ggGAL groups (*n*=2), DSS+SPX1 and DSS+ggSPX2 groups (*n*=3). A: Venn diagram of DEGs among DSS+SPX1, DSS+ggSPX2, and DSS+ggGAL groups. B, C: Heatmap and GSVA scores of immune-related pathways. D, E: Heatmap and GSVA scores of epithelial-related pathways. F: Heatmap of representative DEGs. G: mRNA expression levels of *Il1b*, *Il6*, *Tnfa*, *Ocln*, *Tjp1*, and *Muc2* in colon tissues from DSS-induced colitis mice (*n*=8), measured by RT-qPCR and normalized to *Actb*. H: Western blot and quantification of TJP1 and OCLN in colon tissues. Protein levels were normalized to β-actin (*n*=6 from three independent experiments). I: IHC staining of OCLN and TJP1 and TEM images of colon sections. Black arrows indicate: microvilli (MV), glycocalyx (GL), tight junctions (TJ), mitochondria (M), Golgi apparatus (G), nuclei (N), mucin granules (MG), lysosomes (Ly), and autophagic structures (Au). Scale bars are shown in each panel. Data were analyzed using two-sided Student's *t* test or one-way ANOVA and presented as mean±SEM. ns: Not significant; *: *P*<0.05; **: *P*<0.01; ***: *P*<0.001; ****: *P*<0.0001.

(Figure 2H) and IHC (Figure 2I) confirmed the pronounced upregulation and proper junctional localization of tight junction proteins TJP1 and OCLN following SPX treatment. Ultrastructurally, DSS administration induced severe damage, characterized by disrupted tight junctions, shortened and sparse microvilli, loss of the glycocalyx, increased autophagic vesicles and lysosomes, abnormal nuclear morphology, swollen mitochondria, prominent cytoplasmic vacuolization (Figure 2I, indicated by arrows). Treatment with SPX1 and ggSPX2 peptides significantly attenuated these ultrastructural alterations, demonstrating notably superior restorative efficacy compared to ggGAL. Together, these results demonstrated that SPX alleviates colitis through multiple mechanisms, including immunomodulation, anti-inflammatory responses, and notably, the potent restoration of intestinal epithelial barrier integrity, a feature distinguishing it from GAL.

SPX-activated mammalian GALR2 exhibits G protein-coupling preference

SPX can bind to GALR2/3 but does not activate GALR1 (Duan et al., 2022; Jiang & Zheng, 2022). To identify the target receptor(s) mediating the therapeutic effects of SPX in colitis, we first analyzed the expression of GALR2/3 in human colon tissues from IBD patients and controls yet observed no significant disease-associated trends (Supplementary Figure S6). We therefore compared the signaling profiles of SPX (SPX1 and ggSPX2) and GAL (hsGAL and ggGAL) via GALR2/3 *in vitro*. Strikingly, SPX elicited significantly higher maximal efficacy (E_{max}) than GAL in activating G protein pathways downstream of hsGALR2 (Figure 3A–D). In contrast, GAL showed stronger β-arrestin2 recruitment (Figure 3E). We then calculated the ΔΔlogRAi parameter, which could reflect the differences in the efficacy and potency of different pathways (Zhao et al., 2023) and confirmed that SPX1/2 is distinctly biased toward NFAT-Luc activation over β-arrestin2 recruitment at hsGALR2 compared with GAL (Figure 3F). In parallel with the findings in hsGALR2, mmGALR2 exhibited a similar G-protein bias, along with a minor SRF-Luc response (Figure 3G–L), while no comparable signaling bias was detected for GALR3 (Supplementary Figure S7). The conserved and robust NFAT-Luc activation indicates a preferential coupling of mammalian SPX-GALR2 to Gq, in contrast to a GAL-GALR2-β-arrestin2 bias. This functional divergence highlights receptor- and ligand-specific pathway preferences that may underlie the superior therapeutic efficacy of SPX in mouse colitis.

We next asked whether this signaling bias is evolutionarily conserved. In avian receptors, functional divergence was evident: ggGALR2 responded more strongly to GAL across both G-protein and β-arrestin2 pathways, whereas ggGALR2b and ggGALR3 displayed reversed ligand specificity, with SPX showing higher potency (lower EC_{50}) in all pathways tested (Supplementary Figure S8). This functional divergence between avian and mammalian GALR2 receptors may stem from limited sequence identity between hsGALR2 and ggGALR2 (63%) or ggGALR2b (56%), and this signaling bias variation may play a functional role in avian evolution, warranting future investigation.

SPX alleviates colitis mainly via GALR2 activation

We hypothesized that the Gq-biased signaling of SPX at mammalian GALR2 may account for its enhanced therapeutic efficacy against mouse colitis. First, to identify the target receptor, we utilized *Galr2*$^{-/-}$and *Galr3*$^{-/-}$ mice in established DSS and TNBS-induced colitis models. After seven days of 2% DSS administration, mice displayed colitis of comparable severity, and SPX1 treatment remained effective in *Galr3*$^{-/-}$ mice (though reduced versus WT mice), while its efficacy was markedly attenuated in *Galr2*$^{-/-}$ mice (Figure 4A–J). This receptor-specific dependency was further validated in TNBS-induced colitis, where *Galr2* ablation substantially impaired SPX1 activity, whereas *Galr3* deficiency only marginally affected treatment outcomes (Supplementary Figure S9). Parallel experiments with ggSPX2 in the DSS model demonstrated a conserved reliance on GALR2, regardless of peptide sequence variation (Supplementary Figure S10). To further validate the roles of the two receptors, we employed selective antagonists M871 (GALR2-specific) (Sollenberg et al., 2006) and SNAP37889 (GALR3-specific) (Ash et al., 2011; Swanson et al., 2005) in DSS models. Mice received daily i.p. injections of antagonists 30 min before peptide treatment, with vehicle controls receiving saline (Figure 4J; Supplementary Figure S11A). Although SPX1 efficacy was reduced in both antagonist-treated groups, the inhibition by M871 was significantly more pronounced. Taken together, these results demonstrated that GALR2 is the primary receptor mediating the therapeutic efficacy of SPX in colitis.

SPX attenuates colitis through epithelial cell-intrinsic Gq-coupled signaling

We next sought to identify the downstream effector protein of the SPX-GALR2 axis in colitis. Based on prior evidence that GALR2 predominantly couples to Gq proteins (Duan et al., 2022; Jiang & Zheng, 2022), consistent with our observed bias toward NFAT-Luc activation, we generated *Gnaq*$^{fl/fl}$ and *Arrb2*$^{fl/fl}$ mice (Supplementary Figure S12). The intestinal epithelium, comprised of absorptive enterocytes, mucus-secreting goblet cells, hormone-producing enteroendocrine cells and proliferative progenitors, forms a critical barrier disrupted in colitis (Peterson & Artis, 2014). Within this compartment, GALR2 was broadly expressed while GALR3 and SPX showed more restricted patterns (Supplementary Figure S6E-G). Having validated the barrier-repair function of SPX, and given the broad epithelial expression of GALR2, we targeted epithelial signaling using an AAV8-Vil-Cre system driven by the villin promoter, an actin-binding protein highly expressed in intestinal microvilli (Arpin et al., 1988; El Marjou et al., 2004; Polyak et al., 2012), to achieve intestinal epithelial-specific knockout of *Gnaq* (*Gnaq*$^{\Delta Vil}$, Figure 5A) and *Arrb2* (*Arrb2*$^{\Delta Vil}$, Figure 5N). After viral administration via enema in 8- to 10-week-old male mice, colitis was induced with 2% DSS one week later. RT-qPCR analysis of colon tissues confirmed efficient knockdown of *Gnaq* and *Arrb2* in colon tissue, with no baseline effects on body weight, colon length, inflammation, or epithelial integrity (Supplementary Figure S12).

Upon DSS challenge, *Gnaq*$^{\Delta Vil}$ mice displayed exacerbated disease severity, and the therapeutic benefit of SPX1 was markedly diminished in these mice, as reflected in impaired recovery of body weight, aggravated colon shortening, heightened inflammatory responses, and compromised barrier function. In contrast, ggGAL treatment retained its protective efficacy (Figure 5B–M). *Arrb2*$^{\Delta Vil}$ mice also developed more severe colitis, while SPX1 treatment retained significant therapeutic efficacy, but GAL-mediated protection was almost completely abolished (Figure 5O–Z). These results suggested that SPX alleviates colitis primarily through epithelial cell-

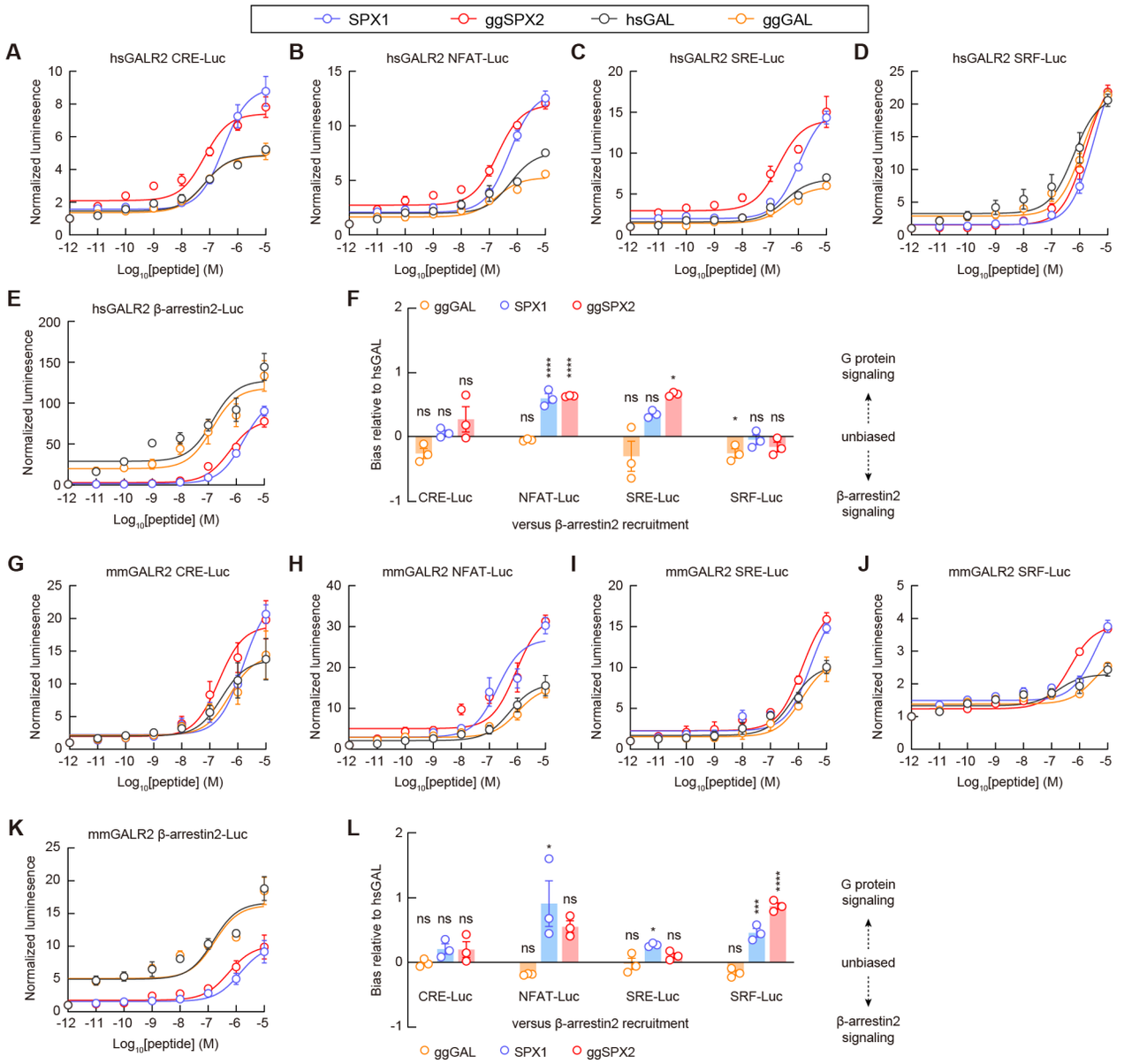

Figure 3 SPX exhibits G protein-coupling bias over β-arrestin2 recruitment at mammalian GALR2

A–D: Activation of CRE-Luc (A), NFAT-Luc (B), SRE-Luc (C), and SRF-Luc (D) downstream of hsGALR2 by tetrapod SPX1, ggSPX2, hsGAL, and ggGAL, measured by luciferase reporter assays. E: β-arrestin2 recruitment downstream of hsGALR2, measured by Tango assay. F: Bias factors of ggGAL, SPX1, and ggSPX2 relative to hsGAL at hsGALR2. Factor>0 indicates a bias towards G protein signaling; factor<0 indicates a bias towards β-arrestin2 signaling. G–J: Activation of CRE-Luc (G), NFAT-Luc (H), SRE-Luc (I), and SRF-Luc (J) downstream of mouse GALR2 (mmGALR2). K: β-arrestin2 recruitment downstream of mmGALR2. L: Bias factors of ggGAL, SPX1, and ggSPX2 relative to hsGAL at mmGALR2. Data were analyzed using one-way ANOVA and presented as mean±SEM. ns: Not significant; *: P<0.05; ***: P<0.001; ****: P<0.0001.

intrinsic Gq activation, whereas GAL-mediated protection appeared contingent upon β-arrestin2 signaling cascades.

Key residues of SPX for regulating Gq signaling bias

Having established the central role of the SPX-GALR2-Gq axis in colitis amelioration, we sought to decipher the structural determinants underlying the distinct signaling profiles of SPX and GAL. Crystal structures of hsGALR2 in complex with SPX1 or hsGAL revealed highly similar binding modes, with only the N-terminal 13 residues of each ligand engaging the receptor (Supplementary Figure S13A, B) (Jiang & Zheng, 2022). We therefore speculated that sequence variations within this region drive functional bias. SPX1 differed from hsGAL at positions 1, 4–8, 11, 13, and 14, which showed signatures of positive selection (excluding residues 13 and 14) (Figure 6A; Supplementary Figure S13C, D). Prior work indicated that substituting SPX1 residues with GAL counterparts (Q5N, M7A, K11F/L, A13P) reduced GALR3-driven SRE-Luc activity in HEK293-Gqi cells, while the L8G substitution impaired activation of both GALR2 and GALR3 (Jiang & Zheng, 2022). Building on this, we introduced Q5N, M7A, L8G, K11L, and A13P substitutions into SPX1 and evaluated their effects on GALRs signaling. These mutations consistently lowered the E_{max} for CRE-Luc, NFAT-Luc, SRE-Luc and SRF-Luc activation via hsGALR2 and mmGALR2, while modestly enhancing β-arrestin2 recruitment (except L8G) (Figure 6B–E; Supplementary Figure S14). In contrast, signaling through hsGALR3, mmGALR3, and ggGALR2/2b/3 remained largely unaffected (Supplementary Figure S15).

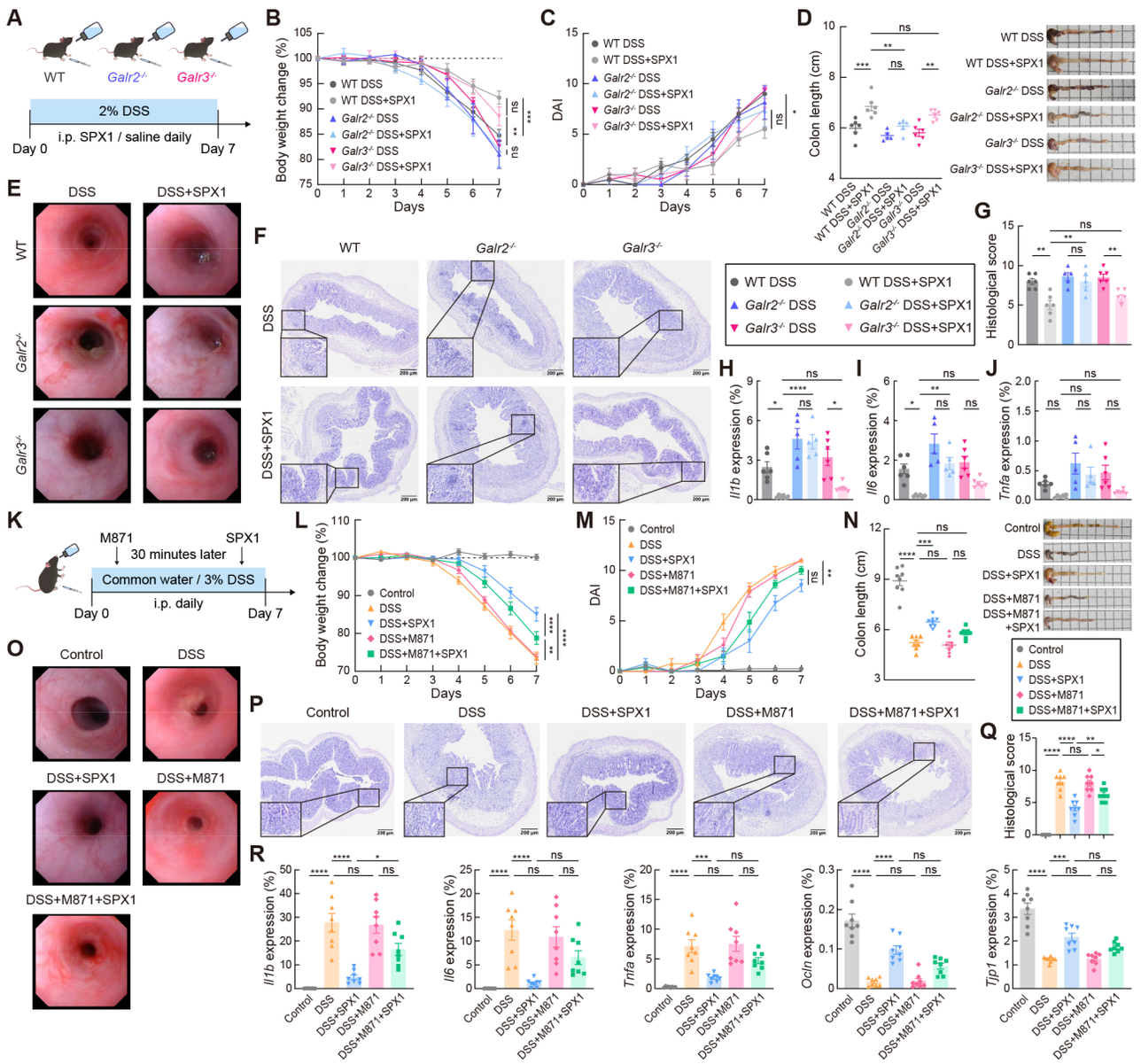

Figure 4 SPX ameliorates colitis primarily via GALR2 activation

A–J: SPX1 treatment in WT, *Galr2*$^{-/-}$, and *Galr3*$^{-/-}$ mice with DSS-induced colitis. A: Flowchart of mouse model. WT (*n*=6, each), *Galr2*$^{-/-}$ (*n*=5, each), and *Galr3*$^{-/-}$ (*n*=6, each) mice were administered 2% DSS. K–R: Co-administration of SPX1 and GALR2 inhibitor M871 in 3% DSS-induced colitis. K: Flowchart of mouse model (*n*=8, each). M871-treated groups additionally received daily i.p. injections of antagonist solution. B, L: Daily body weight changes. C, M: Daily DAI scores. Statistical significance for day 7 is indicated. D, N: Colon length and colon images. E, O: Colonoscopy images. F, P: H&E staining of colon sections. G, Q: Histological scores of H&E-stained colon sections. H–J: mRNA expression levels of *Il1b* (H), *Il6* (I), and *Tnfa* (J) in colon tissues, measured by RT-qPCR and normalized to *Actb*. R: mRNA expression levels of *Il1b*, *Il6*, *Tnfa*, *Ocln*, and *Tjp1* in colon tissues. Data were analyzed using one-way or two-way ANOVA and presented as mean±SEM. ns: Not significant; *: *P*<0.05; **: *P*<0.01; ***: *P*<0.001; ****: *P*<0.0001.

Together, these findings highlighted residues 5, 7, 8, and 11 of mature SPX as critical modulators of Gq signaling bias.

SPX p.Lys11Leu, a high-affinity GALR2 ligand, holds therapeutic promise in colitis

Among the variants tested, the p.Lys11Leu (SPX^{K11L}) mutant exhibited markedly increased potency in activating multiple downstream pathways of hsGALR2 and mmGALR2 (Figure 6B–E, Supplementary Figure S14). Using BRET2 (Olsen et al., 2020) and MeNArc2 (Hauge Pedersen et al., 2021) assays, we confirmed that SPX1^{K11L} can more efficiently promote Gαq-βγ subunit dissociation and β-arrestin2 recruitment (Figure 6F, G). Crystal structures indicated that L11 of GAL contributed to a hydrophobic microdomain on GALR2, formed by TM6 (L255, I256, V259), ECL3 (F264, L266), and TM7 (Y271), with R184 of GALR2 forming a hydrogen bond with the main chain carbonyl of L11 (Duan et al., 2022). To probe the SPX1^{K11L}-GALR2 interface, we engineered a series of hsGALR2 mutants (R184A/E, V259A/E/R, L266A/E/R) (Figure 6H, I; Supplementary Figure S16) and corresponding mmGALR2 mutants (R183A/E, V258A/E/R, L265A/E/R) (Supplementary Figure S17). In G protein signaling, mutations at these sites variably reduced the E_{max} for SPX1-mediated activation. The R184A mutation abolished the left-shift in EC_{50} conferred by p.Lys11Leu, restoring it to SPX1-like levels, whereas R184E nearly

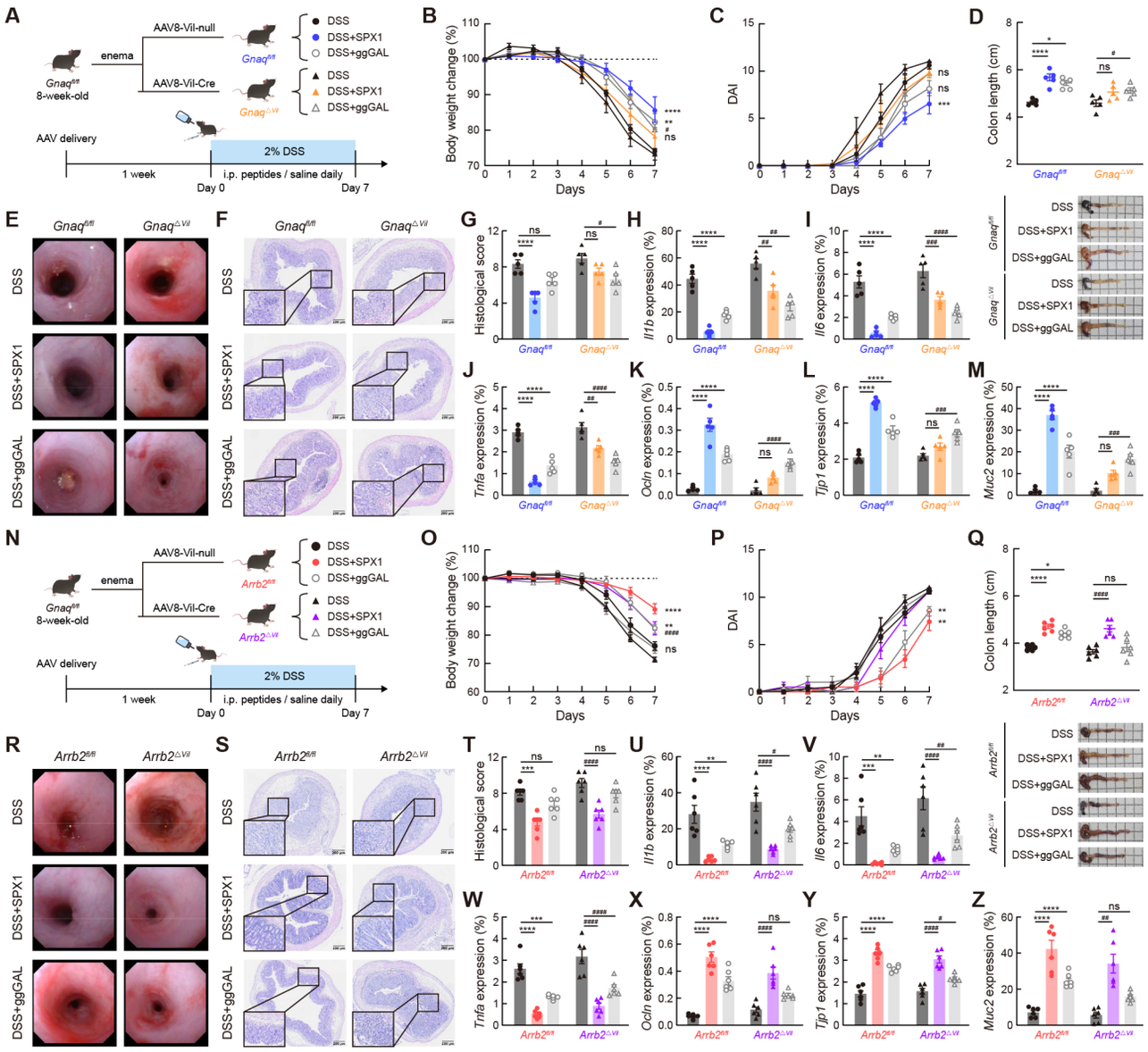

Figure 5 SPX treatment for colitis depends on epithelial cell-intrinsic Gq signaling

A–M: SPX1 administration in *Gnaq*$^{fl/fl}$ and *Gnaq*$^{\triangle Vil}$ mice with 2% DSS-induced colitis. N–Z: SPX1 administration in *Arrb2*$^{fl/fl}$ and *Arrb2*$^{\triangle Vil}$ mice with DSS-induced colitis. A, N: Flowchart of mouse model. Floxed mice received a rectal administration of AAV8-Vil-null (*Gnaq*$^{fl/fl}$ or *Arrb2*$^{fl/fl}$) or AAV8-Vil-Cre virus to achieve specific knockout of *Gnaq* or *Arrb2* in intestinal epithelial cells (*Gnaq*$^{\triangle Vil}$ or *Arrb2*$^{\triangle Vil}$). One week later, mice were randomly divided into Control (Supplementary Figure S12), DSS, DSS+SPX1, and DSS+ggGAL groups (for *Gnaq* mice, n=5, each; for *Arrb2* mice, n=6, each). B, O: Daily body weight changes. C, P: Daily DAI scores. Statistical significance for day 7 is indicated. D, Q: Colon length and colon images. E, R: Colonoscopy images. F, S: H&E staining of colon sections. G, T: Histological scores of H&E-stained colon sections. H–M: mRNA expression levels of *Il1b*, *Il6*, *Tnfa*, *Ocln*, *Tjp1*, and *Muc2* in colon tissues from *Gnaq* mice, measured by RT-qPCR and normalized to *Actb*. U–Z: mRNA expression levels of *Il1b*, *Il6*, *Tnfa*, *Ocln*, *Tjp1*, and *Muc2* in colon tissues from *Arrb2* mice. Data were analyzed using one-way or two-way ANOVA and presented as mean±SEM. * indicates significance compared to AAV8-Vil-null group; # indicates significance compared to AAV8-Vil-Cre group. ns: Not significant; *: P<0.05; **: P<0.01; ***: P<0.001; ****: P<0.0001.

abolished receptor activation, which underscored the essential role of R184 in ligand engagement. The V259A/E and L266A/E/R mutations modestly increased EC_{50} values for SPX1^{K11L}, suggesting that the pLys11Leu substitution optimized hydrophobic complementarity within this conserved microdomain. Intriguingly, V259R did not alter EC_{50} significantly, while V259A/R and L266R enhanced β-arrestin2 recruitment (Supplementary Figure S16), hinting at conformational adjustments that favor β-arrestin2–biased signaling. These data implied that the enhanced potency of SPX1^{K11L} may stem from synergistic optimization of both hydrophobic interface stabilization (TM6/ECL3) and polar anchoring (R184-ECL2).

We next assessed the therapeutic potential of SPX p.Lys11Leu peptide in DSS-induced colitis (Figure 7). Two concentrations were tested: 0.5 μmol/L (approximately the EC_{50} of SPX1, Supplementary Table S5) and 3 μmol/L (the original concentration used for SPX1) (Figure 7A). While 3 μmol/L SPX1 remained therapeutic, 0.5 μmol/L SPX1 showed negligible activity (Figure 7B–L). Strikingly, 0.5 μmol/L SPX1^{K11L} achieved therapeutic efficacy comparable to 3 μmol/L SPX1, indicating that the increased potency

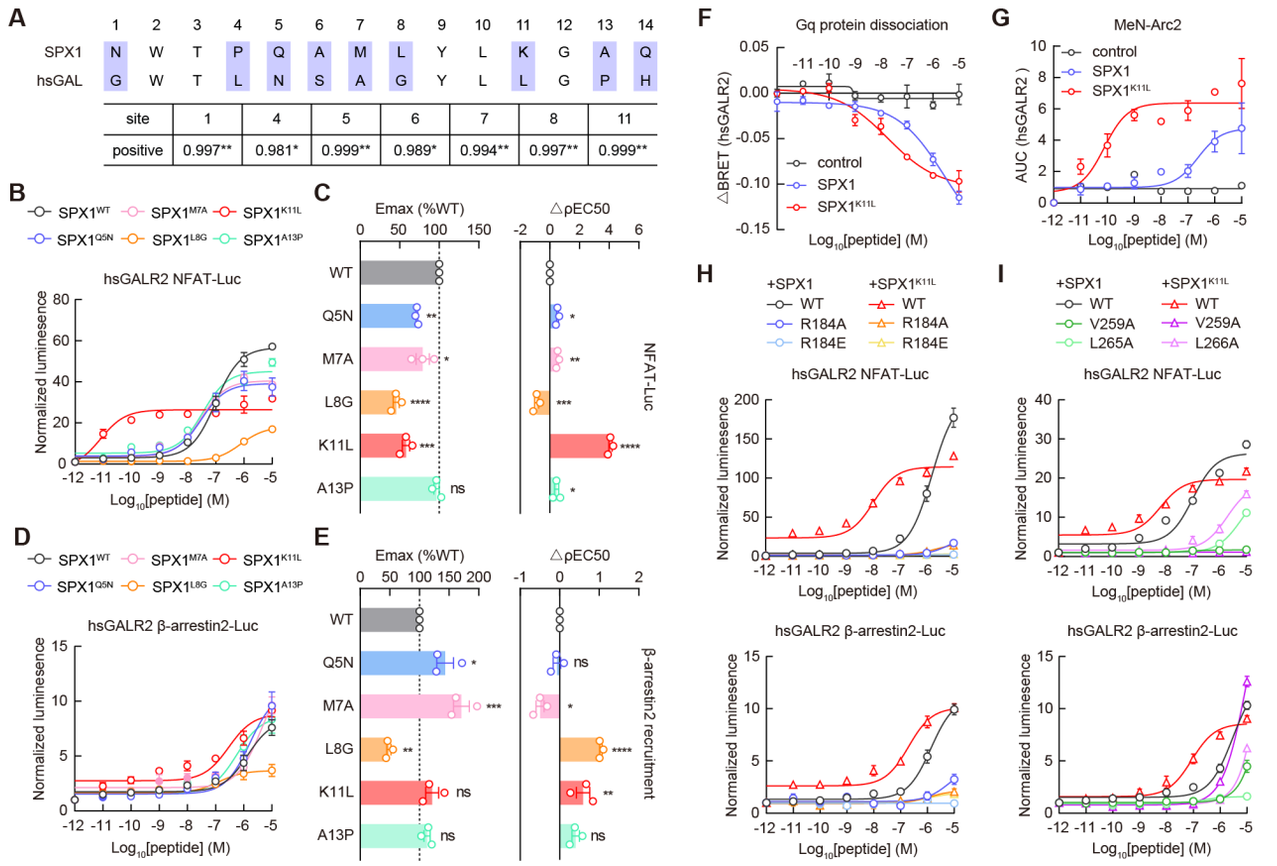

Figure 6 Contribution of pocket residues to SPX-induced Gq signaling bias

A: Sequence alignment of SPX1 and the first 14 amino acids of hsGAL mature peptide. Boxes indicate different residues. The table shows positively selected sites identified by branch-site model analysis (Supplementary Figure S13). * indicates BEB posterior probabilities＞0.95. B, C: Effects of SPX1 mutants on NFAT-Luc activation downstream of hsGALR2. B: Dose-response curves. C: E_{max} (% of WT SPX1) and ΔpEC_{50} (mutant pEC_{50}–WT pEC_{50}). D, E: Effects of SPX1 mutants on β-arrestin2 recruitment downstream of hsGALR2. D: Dose-response curves. E: E_{max} (% of WT SPX1) and ΔpEC_{50}. F: $SPX1^{K11L}$ reduced the EC_{50} of hsGALR2 for Gαq-βγ dissociation detected by BRET2 assay. G: $SPX1^{K11L}$ reduced the EC_{50} of hsGALR2 for β-arrestin2 recruitment detected by MeN-Arc2 system. H, I: R184A/E and V259A/L266A mutants of hsGALR2 impair interaction with $SPX1^{K11L}$. Data were analyzed using one-way ANOVA and presented as mean±SEM. ns: Not significant; *: P<0.05; **: P<0.01; ***: P<0.001; ****: P<0.0001.

conferred by the pLys11Leu mutant enabled efficacy at a substantially lower dose. Thus, $SPX1^{K11L}$ emerged as a high-affinity GALR2 ligand with potential for improved colitis therapy through dose-sparing effects, exemplifying a rational design approach for optimizing GALR2-targeted drugs.

DISCUSSION

IBD persists as a formidable therapeutic challenge, compelling the exploration of innovative treatment strategies (Kaplan, 2015; Massironi et al., 2023). Building on prior investigations that identified galanin (GAL) as a potential therapeutic agent in IBD (Bauer et al., 1989; Lai et al., 2025; Talero et al., 2006), we adopted an evolutionary perspective through Darwinian medicine principles, which seeks to understand diseases through an evolutionary lens (Natterson-Horowitz et al., 2023; Stearns & Ebert, 2001; Williams & Nesse, 1991), to explore the therapeutic promise of spexin (SPX), an evolutionary relative of GAL (Kim et al., 2014; Mills et al., 2021). Our research elucidates the evolutionary trajectory of SPX, establishes its efficacy in suppressing inflammation and restoring epithelial barrier integrity in colitis, and identifies the SPX-GALR2-Gq signaling axis as a critical mechanistic pathway, offering a novel therapeutic direction for colitis management.

SPX, a 14-amino-acid mature neuropeptide originating in cartilaginous fish, displays notable evolutionary dynamics and sequence variation (Supplementary Figure S1). While non-mammalian vertebrates possessed two paralogs (*SPX1* and *SPX2*), *SPX2* was lost in mammals (Kim et al., 2014) and several avian lineages (*Anseriformes*, *Cuculiformes*, *Columbiformes*, *Charadriiformes*, and *Passeriformes*) (Supplementary Figure S2), suggesting relaxed selective constraints in these groups. SPX shares galanin receptors (GALRs) with GAL. The GALR family consists of GALR1, GALR2, and GALR3, all of which are G protein-coupled receptors (GPCRs) (Branchek et al., 2000). GALRs also exhibit considerable evolutionary plasticity, exemplified by the presence of GALR1a/1b and GALR2a/2b in fish, while GALR3 is absent; amphibians and birds possess GALR2a/2b, whereas mammals have a single copy of each GALR subtype (Kim et al., 2014). This co-evolutionary history makes the SPX-GALR system a compelling model for Darwinian medicine.

As a pleiotropic neuropeptide broadly expressed in both the central nervous system and peripheral tissues, SPX has demonstrated notable anti-inflammatory properties, including in metabolic disorders (Lv et al., 2019). A recent report

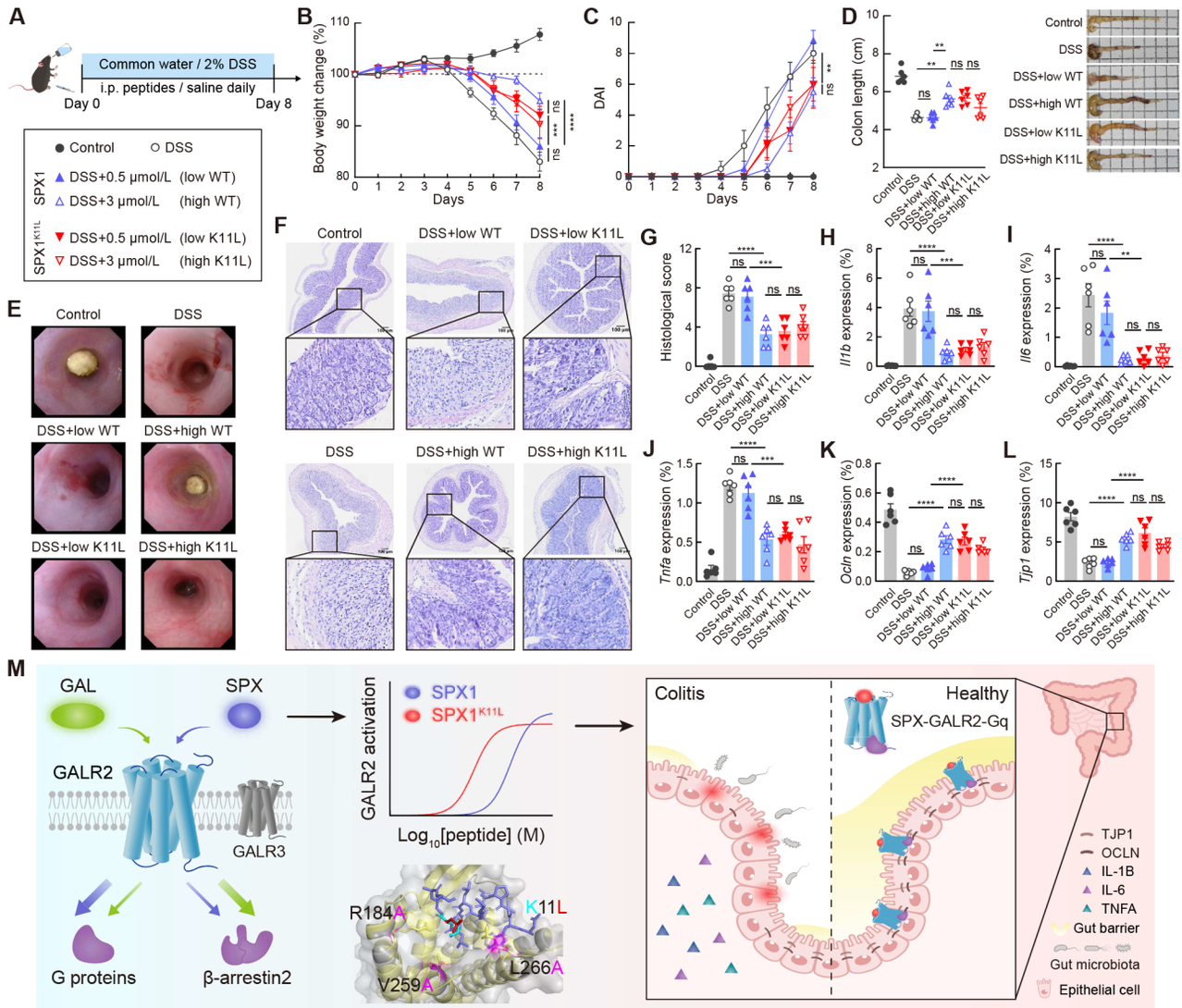

Figure 7 SPX^{K11L} mutant demonstrates potent therapeutic efficacy for colitis at lower concentrations

A: Flowchart of 2% DSS-induced colitis mouse model. 8-week-old male mice were randomly divided into groups (n=6, each): Control, DSS, DSS+0.5 μmol/L SPX1 (low WT), DSS+3 μmol/L SPX1 (high WT), DSS+0.5 μmol/L SPX1^{K11L} (low K11L), and DSS+3 μmol/L SPX1^{K11L} (high K11L). B: Daily body weight changes. C: Daily DAI scores. Statistical significance for day 8 is indicated. D: Colon length and colon images. E: Colonoscopy images. F: H&E staining of colon sections. G: Histological scores of H&E-stained colon sections. H–L: mRNA expression levels of *Il1b*, *Il6*, *Tnfa*, *Ocln*, and *Tjp1*, measured by RT-qPCR and normalized to *Actb*. M: Schematic illustration of SPX-GALR2-Gq signaling axis in colitis therapy. Left: SPX acts as a biased GALR2 agonist, preferentially activating Gq signaling over β-arrestin2 recruitment, which is favored by GAL. Middle: SPX p.Lys11Leu mutant exhibits enhanced GALR2 affinity, potentially via altered binding at R184 and stabilization of the V259 (TM6)/L266 (ECL3) hydrophobic interface. Right: SPX1^{K11L} reduces inflammatory cytokines and promotes intestinal barrier restoration in colitis. Data were analyzed using one-way or two-way ANOVA and presented as mean±SEM. ns: Not significant; *: P<0.05; **: P<0.01; ***: P<0.001; ****: P<0.0001.

indicated that SPX attenuates acetic acid-induced colitis in rats by modulating the NF-κB/NLRP3 signaling cascade, mitigating oxidative damage, enhancing antioxidant defenses, and suppressing inflammatory responses (Tamer et al., 2025). In our study, exogenous SPX1/2 administration significantly attenuated both DSS- and TNBS-induced colitis (Figure 1). Notably, both SPX1 (identical sequences in human, mouse, and chicken) and chicken SPX2 (ggSPX2) exhibited superior efficacy compared to GAL in colitis models (Figure 1), underscoring its fundamental role in intestinal homeostasis. While *in vitro* assessment of SPX2 orthologs from several species, including green anole, zebrafish, and medaka, did not reveal any with markedly enhanced potency (Supplementary Figure S3), this remains a fertile area for future exploration.

Mechanistically, SPX treatment significantly inhibited inflammation and reduced pro-inflammatory cytokine production in mouse colitis (Figure 2). Beyond its anti-inflammatory effects, SPX actively fortified the intestinal epithelial barrier, as evidenced by increased expression of tight junction proteins (TJP1, OCLN), ultrastructural improvements in junctional morphology, and enhanced microvilli density via TEM. SPX also upregulated *Muc2* expression in colon tissues (Figure 2), a critical component for intestinal mucus secretion and barrier function (Luis & Hansson, 2023), and modulated intestinal stem cell dynamics, altering the expression of key regulators (*Lgr5*, *Sox9*), proliferative markers (*Mki67*, *Myc*), and differentiation mediators (*Atoh1*, *Gata6*) (Figure 2) (Yeung et al., 2011). This comprehensive repair capacity positions SPX as a key coordinator for epithelial and mucosal restoration. The integrity

of the intestinal barrier, a complex structure comprising the mucus layer and a dynamic epithelial monolayer constantly renewed from ISCs, is paramount for homeostasis (Peterson & Artis, 2014). Single-cell expression analysis revealed that GALR2, the primary receptor mediating the effect of SPX, was broadly distributed across colonic epithelial lineages, including mucus-secreting goblet cells, absorptive enterocytes, and undifferentiated cells, while SPX was notably expressed in undifferentiated cell populations (Supplementary Figure S6). This complementary expression pattern suggests that SPX-GALR2 signaling may function in a paracrine or autocrine manner to locally regulate epithelial repair programs.

SPX selectively activates GALR2 and GALR3, but not GALR1 (Duan et al., 2022; Jiang & Zheng, 2022). GALR2 couples to both G proteins and β-arrestin1/2 pathways, and SPX-bound GALR2 shows only modest β-arrestin2 recruitment compared to GAL (Reyes-Alcaraz et al., 2018), whereas GALR3 mainly binds to Gi/o proteins to lower cAMP levels (Duan et al., 2022; Jiang & Zheng, 2022). SPX-GALR2 signaling has been shown to modulate gut motility via L-type VDCCs (Lin et al., 2015) and to reduce atrial fibrillation susceptibility by inhibiting CREB phosphorylation in mice (Li et al., 2024). Our study is the first to confirm the key role of the SPX-GALR2 signaling axis in colitis. *In vitro*, luciferase reporter assays confirmed that SPX-activated GALR2 exhibited a pronounced bias toward G protein-coupled pathways (particularly NFAT-Luc activation) over β-arrestin2 recruitment, a profile distinct from that of GAL (Figure 3). This signaling bias was evolutionarily conserved in mammalian receptors but showed interesting divergence in non-mammalian vertebrates, where ggGALR2b/3 were preferentially activated by SPX, but ggGALR2 displayed a higher affinity for GAL across all signaling pathways (Supplementary Figure S8). These results demonstrated evolutionary divergence in signal transduction among GALR subtypes, potentially reflecting adaptive tuning of neuroendocrine regulation associated with the GALRs-SPX/GAL system across vertebrates. *In vivo*, we utilized *Galr2*$^{-/-}$ and *Galr3*$^{-/-}$ mice, together with selective inhibitors for GALR2 (M871) (Sollenberg et al., 2006) and GALR3 (SNAP37889) (Swanson et al., 2005), to consolidate the role of GALR2 in SPX-mediated efficiency in colitis. Previous reports indicated exacerbated DSS-induced colitis in *Galr3*$^{-/-}$ mice, but not *Galr2*$^{-/-}$ mice, compared to WT controls, prompting us to adopt the 2% DSS protocol (Brunner et al., 2021) instead of our usual 3%. However, we did not observe the exacerbated colitis in *Galr2*$^{-/-}$ and *Galr3*$^{-/-}$ mice (Figure 4; Supplementary Figure S9), a discrepancy potentially attributable to differences in genetic background (C57BL/6N in the previous study (Brunner et al., 2021) vs. C57BL/6JGpt in our study). We also observed that mammalian GALR3 showed less pronounced signaling under SPX/GAL treatment (Supplementary Figure S7). This may be due to methodological limitations within our detection system, which may not fully capture the intensity of GALR3 downstream signaling, potentially underestimating its activation compared to other approaches (Kim et al., 2014). Even though GALR3 appeared to act less prominently in SPX-mediated colitis therapy, elucidating the SPX-GALR3 signaling axis and its potential physiological roles remains a valuable avenue for future research.

GALR2 primarily couples with Gq/11 protein to activate phospholipase C signaling, thereby elevating intracellular calcium concentrations (Duan et al., 2022; Jiang & Zheng, 2022). Our luciferase reporter assays further revealed that SPX-activated hsGALR2 and mmGALR2 exhibited significant biased signaling toward the NFAT-Luc pathway. Therefore, to dissect the downstream effector pathway, we generated conditional *Gnaq* and *Arrb2* knockout mice. Given the expression pattern of GALR2 in the colon, and the observed restorative effects of SPX on intestinal barrier function, we employed an adeno-associated virus (AAV) carrying *Villin-Cre* (Arpin et al., 1988; El Marjou et al., 2004; Polyak et al., 2012). Both *Gnaq*$^{\Delta Vil}$ and *Arrb2*$^{\Delta Vil}$ mice exhibited aggravated colitis upon DSS challenge (Figure 5), consistent with the established roles of *Gnaq* and *Arrb2* in intestinal homeostasis (Sharma et al., 2015; Watanabe et al., 2016; Zeng et al., 2015). The therapeutic efficacy of SPX was substantially abrogated in *Gnaq*$^{\Delta Vil}$ mice but preserved in *Arrb2*$^{\Delta Vil}$ mice, whereas GAL-mediated protection showed the exact opposite dependence, being lost in *Arrb2*$^{\Delta Vil}$ mice (Figure 5). These results establish that SPX alleviates colitis primarily through epithelial-intrinsic Gq activation, while GAL operates via β-arrestin2. Importantly, the residual efficacy of SPX in *Gnaq*$^{\Delta Vil}$ mice suggests the possible involvement of complementary mechanisms (Figure 5), such as immunomodulation via GALR2-expressing T-cells (Supplementary Figure S6) or engagement of alternative G proteins, which was not fully assessed here. Furthermore, although *Villin-Cre* effectively targets intestinal epithelia, its limited cellular resolution precludes discrimination of specific lineages. Future studies employing *Lgr5*- or *Muc2*-driven targeting strategies to selectively modulate intestinal stem cells (given the impact of SPX on proliferation/differentiation) or goblet cells (given the SPX-induced MUC2 upregulation), respectively, are warranted to delineate the precise cellular mechanisms underlying the therapeutic efficacy of SPX in colitis.

Beyond local intestinal inflammation, dysregulation of the gut-brain axis is increasingly implicated in IBD. Chronic gut inflammation alters microbiota composition (Ni et al., 2017), potentially impairing gut-brain communication and exacerbating anxiety/depressive-like behaviors via neuroimmune activation (Bisgaard et al., 2022), and such neurological-enteric interactions create a self-perpetuating inflammatory cycle, further diminishing the overall quality of life for patients. Intriguingly, SPX has demonstrated anxiolytic and antidepressant potential (Lv et al., 2019), and SPX-based GALR2 agonists can significantly alleviate anxiety-like behaviors in mice (Reyes-Alcaraz et al., 2016). Moreover, combination of a high-fiber diet and the starch blocker acarbose ameliorates polycystic ovary syndrome (PCOS) symptoms, accompanied by shifts in gut microbiota composition and elevated SPX levels (Wang et al., 2022), suggesting a potential role for SPX in gut-brain communication. Although the mental aspects of mice were not tested in our study, it is plausible that SPX could simultaneously ameliorate intestinal inflammation and mood disturbances in IBD, a promising avenue for future research.

A single GPCR can orchestrate diverse physiological functions by engaging distinct downstream signaling cascades (Whalen et al., 2011; Wootten et al., 2018). For example, the angiotensin II receptor type 1 (AT1R) elevates blood pressure via Gq/11 signaling (Forrester et al., 2018), while β-arrestin2 activation contributes to cardiovascular remodeling (Fu et al., 2021), and β-arrestin-biased ligands, such as TRV027, competitively bind AT1R to mitigate deleterious effects (Violin

et al., 2014). Similarly, the μ-opioid receptor (MOR) elicits analgesia through Gi/o signaling (Koehl et al., 2018), while concurrent β-arrestin recruitment leads to respiratory depression (Che & Roth, 2023), driving the development of G protein-biased ligands like oliceridine (TRV130), designed to provide analgesia with diminished side effects (Violin et al., 2014). In our study, we observed a trend of increased SPX expression in UC and decreased expression in CD, however, given the potential influence of dynamic disease stage variations and methodological limitations, further validation is warranted. Furthermore, analysis of GALR2/3 expression patterns in IBD patient cohorts did not differ significantly (Supplementary Figure S6), suggesting that the therapeutic benefits from the SPX-GALR2-Gq axis in colitis indicate its potential clinical relevance through pathway modulation rather than receptor abundance alterations, analogous to the successful biased drug therapies.

To elucidate the mechanism by which SPX activates G protein bias downstream of GALR2, we analyzed crystal structures of GALR2 (PDB: 7XJK, 7WQ4, 7XBD, 7XJL). SPX engages GALR2 primarily through its N-terminal 13 amino acids, aligning with the binding mode of hsGAL (Supplementary Figure S13) (Jiang & Zheng, 2022; Wong et al., 2021). Mutating SPX at positions 5, 7, 8, and 11 to GAL-like residues significantly impaired Gq signaling via mammalian GALR2 but had no effect on GALR3 and non-mammalian receptors (Figure 6; Supplementary Figures S14–S15), highlighting these residues as key determinants of receptor selectivity and signaling bias. Strikingly, the SPX p.Lys11Leu mutant exhibited enhanced affinity for hsGALR2 and mmGALR2 (Figure 6), translating to superior therapeutic efficacy in DSS-induced colitis at a low concentration, a property not observed in unmodified SPX1 (Figure 7). The molecular surface of SPX was largely hydrophobic with K11 as the only charged residue in the α-helix (Wong et al., 2021), so we hypothesize that the p.Lys11Leu substitution, by eliminating a positive charge, alleviates electrostatic repulsion with R184 and optimizes hydrophobic interactions within the TM6/ECL3/TM7 network, thereby increasing affinity (Figure 6; Supplementary Figure S16–S17). The strict conservation of K/R at position 11 in vertebrate SPX, contrasting with the absence of naturally occurring L substitutions (Supplementary Figure S13), underscores the critical role of this residue in SPX function and its divergence from GAL. These hypotheses need to be further validated with crystal structure data, and continued investigation into the SPX-GALR2-Gq bias regulatory mechanism may unveil additional critical determinants beyond the SPX p.Lys11Leu site, potentially paving the way for the rational design of novel biased drug therapies.

In summary, our study identifies SPX and its SPX1^{K11L} mutant as Gq-biased GALR2 agonists that mitigate inflammation and promote epithelial repair, thereby providing a novel targeted strategy for colitis therapy.

DATA AVAILABILITY

The RNA-sequencing data generated in this study have been deposited in NCBI (BioProject: PRJNA1434174 and PRJNA1334145), GSA (BioProject: PRJCA059716) and Science Data Bank (https://cstr.cn/31253.11.sciencedb.j00139.00242).

CONFLICTS OF INTERESTS

The authors declare that they have no competing interests.

AUTHORS' CONTRIBUTIONS

C.D. and S.L. conceptualized the study; J.W.X., T.Z., X.L.K., Y.W.C., K.L.M., and T.Z. performed experiments and analyzed data; K.Z. and J.W.X. analyzed the RNA-seq data; J.W.X. wrote the original manuscript; J.W.X., J.B., S.S.L. and C.D. revised the manuscript. All authors read and approved the final version of the manuscript.

ACKNOWLEDGMENTS

This work was supported by the National Natural Science Foundation of China (32270438, 32170498), the National Key R&D Program of China (2021YFF0702000), the National Science and Technology Major Project (2023ZD0506800), the 1·3·5 Project for Disciplines of Excellence, West China Hospital, Sichuan University (ZYYC21011), the National Clinical Research Center for Geriatrics, West China Hospital, Sichuan University (Z2023JC003), the Science and Technology Department of Sichuan Province (2022YFH0116), the Priority Academic Program Development of Jiangsu Higher Education Institutions, and the "Kunlun Talents" of Qinghai-Top-Notch and Pioneering talent of Innovation and Entrepreneurship. We thank Professor Fei Xu for providing technical support and assistance during data collection at ShanghaiTech University.

REFERENCES

Arijs I, De Hertogh G, Lemaire K, et al. 2009. Mucosal gene expression of antimicrobial peptides in inflammatory bowel disease before and after first infliximab treatment. *PLoS One*, **4**(11): e7984.

Arpin M, Blair L, Coudrier E, et al. 1988. Villin, a specific marker for some epithelia specialized in transport, to study the differentiation of intestinal and kidney cells *in vivo* and in a human colon adenocarcinoma line HT29 in culture. *Molecular Aspects of Medicine*, **10**(3): 257–272.

Ash BL, Zanatta SD, Williams SJ, et al. 2011. The galanin-3 receptor antagonist, SNAP 37889, reduces operant responding for ethanol in alcohol-preferring rats. *Regulatory Peptides*, **166**(1-3): 59–67.

Azimzadeh P, Olson Jr JA, Balenga N. 2017. Reporter gene assays for investigating GPCR signaling. *Methods in Cell Biology*, **142**: 89–99.

Bauer FE, Zintel A, Kenny MJ, et al. 1989. Inhibitory effect of galanin on postprandial gastrointestinal motility and gut hormone release in humans. *Gastroenterology*, **97**(2): 260–264.

Berthelot C, Brunet F, Chalopin D, et al. 2014. The rainbow trout genome provides novel insights into evolution after whole-genome duplication in vertebrates. *Nature Communications*, **5**(1): 3657.

Bisgaard TH, Allin KH, Keefer L, et al. 2022. Depression and anxiety in inflammatory bowel disease: epidemiology, mechanisms and treatment. *Nature Reviews Gastroenterology & Hepatology*, **19**(11): 717–726.

Branchek TA, Smith KE, Gerald C, et al. 2000. Galanin receptor subtypes. *Trends in Pharmacological Sciences*, **21**(3): 109–117.

Brunner SM, Reichmann F, Leitner J, et al. 2021. Galanin receptor 3 attenuates inflammation and influences the gut microbiota in an experimental murine colitis model. *Scientific Reports*, **11**(1): 564.

Che T, Roth BL. 2023. Molecular basis of opioid receptor signaling. *Cell*, **186**(24): 5203–5219.

Chen XJ, Feng YY, Dai SD, et al. 2024. Advances in research on spexin-mediated regulation of reproductive function in vertebrates. *Frontiers in Endocrinology*, **15**: 1422711.

Cheng ZJ, Garvin D, Paguio A, et al. 2010. Luciferase reporter assay system for deciphering GPCR pathways. *Current Chemical Genomics*, **4**: 84–91.

Cohen Y, Hausken K, Bonfil Y, et al. 2020. Spexin and a novel cichlid-specific spexin paralog both inhibit FSH and LH through a specific galanin receptor (Galr2b) in tilapia. *Frontiers in Endocrinology*, **11**: 71.

Duan J, Shen DD, Zhao TT, et al. 2022. Molecular basis for allosteric agonism and G protein subtype selectivity of galanin receptors. *Nature*

Communications, **13**(1): 1364.

El Marjou F, Janssen KP, Chang BHJ, et al. 2004. Tissue-specific and inducible Cre-mediated recombination in the gut epithelium. *Genesis*, **39**(3): 186–193.

Fang PH, Ge R, She YQ, et al. 2022. Adipose tissue spexin in physical exercise and age-associated diseases. *Ageing Research Reviews*, **73**: 101509.

Fang PH, She YQ, Yu M, et al. 2024. Novel hypothalamic pathways for metabolic effects of spexin. *Pharmacological Research*, **208**: 107399.

Forrester SJ, Booz GW, Sigmund CD, et al. 2018. Angiotensin II signal transduction: an update on mechanisms of physiology and pathophysiology. *Physiological Reviews*, **98**(3): 1627–1738.

Fu Y, Huang YQ, Yang Z, et al. 2021. Cartilage oligomeric matrix protein is an endogenous β-arrestin-2-selective allosteric modulator of AT1 receptor counteracting vascular injury. *Cell Research*, **31**(7): 773–790.

Gao FL, Chen CJ, Arab DA, et al. 2019. EasyCodeML: a visual tool for analysis of selection using CodeML. *Ecology and Evolution*, **9**(7): 3891–3898.

Gonzalez Acera M, Bubeck M, Mascia F, et al. 2021. Dynamic, transient, and robust increase in the innervation of the inflamed mucosa in inflammatory bowel diseases. *Cells*, **10**(9): 2253.

Gu LP, Ma YH, Gu MY, et al. 2015. Spexin peptide is expressed in human endocrine and epithelial tissues and reduced after glucose load in type 2 diabetes. *Peptides*, **71**: 232–239.

Guo SM, Zhao TT, Yun Y, et al. 2022. Recent progress in assays for GPCR drug discovery. *American Journal of Physiology-Cell Physiology*, **323**(2): C583–C594.

Hauge Pedersen M, Pham J, Mancebo H, et al. 2021. A novel luminescence-based β-arrestin recruitment assay for unmodified receptors. *Journal of Biological Chemistry*, **296**: 100503.

Ho JCW, Jacobs T, Wang YJ, et al. 2012. Identification and characterization of the chicken galanin receptor GalR2 and a novel GalR2-like receptor (GalR2-L). *General and Comparative Endocrinology*, **179**(2): 305–312.

Jiang WT, Zheng SD. 2022. Structural insights into galanin receptor signaling. *Proceedings of the National Academy of Sciences of the United States of America*, **119**(21): e2121465119.

Kaplan GG. 2015. The global burden of IBD: from 2015 to 2025. *Nature Reviews Gastroenterology & Hepatology*, **12**(12): 720–727.

Kim DK, Yun S, Son GH, et al. 2014. Coevolution of the spexin/galanin/kisspeptin family: spexin activates galanin receptor type II and III. *Endocrinology*, **155**(5): 1864–1873.

Koehl A, Hu HL, Maeda S, et al. 2018. Structure of the μ-opioid receptor-G_i protein complex. *Nature*, **558**(7711): 547–552.

Kroeze WK, Sassano MF, Huang XP, et al. 2015. PRESTO-Tango as an open-source resource for interrogation of the druggable human GPCRome. *Nature Structural & Molecular Biology*, **22**(5): 362–369.

Kumar S, Stecher G, Li M, et al. 2018. MEGA X: molecular evolutionary genetics analysis across computing platforms. *Molecular Biology and Evolution*, **35**(6): 1547–1549.

Lai SS, Kong XL, Xue JW, et al. 2025. A novel long-galanin peptide from non-mammalian vertebrates mitigates the inflammatory response in IBD models via the biased GALR2/β-arrestin2 pathway. *Nature Communications*, **16**(1): 11512.

Li DS, Liu Y, Li CZ, et al. 2024. Spexin diminishes atrial fibrillation vulnerability by acting on galanin receptor 2. *Circulation*, **150**(2): 111–127.

Lim CH, Lee MYM, Soga T, et al. 2019. Evolution of structural and functional diversity of spexin in mammalian and non-mammalian vertebrate species. *Frontiers in Endocrinology*, **10**: 379.

Lin CY, Zhang M, Huang T, et al. 2015. Spexin enhances bowel movement through activating L-type voltage-dependent calcium channel via galanin receptor 2 in mice. *Scientific Reports*, **5**(1): 12095.

Liu B, Wu DQ. 2004. Analysis of the coupling of G12/13 to G protein-coupled receptors using a luciferase reporter assay. *Methods in Molecular Biology*, **237**: 145–149.

Luis AS, Hansson GC. 2023. Intestinal mucus and their glycans: a habitat for thriving microbiota. *Cell Host & Microbe*, **31**(7): 1087–1100.

Lv SY, Zhou YC, Zhang XM, et al. 2019. Emerging roles of NPQ/spexin in physiology and pathology. *Frontiers in Pharmacology*, **10**: 457.

Marrero JA, Matkowskyj KA, Yung K, et al. 2000. Dextran sulfate sodium-induced murine colitis activates NF-κB and increases galanin-1 receptor expression. *American Journal of Physiology-Gastrointestinal and Liver Physiology*, **278**(5): G797–G804.

Massironi S, Viganò C, Palermo A, et al. 2023. Inflammation and malnutrition in inflammatory bowel disease. *The Lancet Gastroenterology & Hepatology*, **8**(6): 579–590.

Meng FY, Wu YP, Yu Y, et al. 2023. *Spexin2* is a novel food regulator in *Gallus gallus*. *International Journal of Molecular Sciences*, **24**(5): 4821.

Mills EG, Izzi-Engbeaya C, Abbara A, et al. 2021. Functions of galanin, spexin and kisspeptin in metabolism, mood and behaviour. *Nature Reviews Endocrinology*, **17**(2): 97–113.

Natterson-Horowitz B, Aktipis A, Fox M, et al. 2023. The future of evolutionary medicine: sparking innovation in biomedicine and public health. *Frontiers in Science*, **1**: 997136.

Ni J, Wu GD, Albenberg L, et al. 2017. Gut microbiota and IBD: causation or correlation?. *Nature Reviews Gastroenterology & Hepatology*, **14**(10): 573–584.

Olsen J, Gerds TA, Seidelin JB, et al. 2009. Diagnosis of ulcerative colitis before onset of inflammation by multivariate modeling of genome-wide gene expression data. *Inflammatory Bowel Diseases*, **15**(7): 1032–1038.

Olsen RHJ, DiBerto JF, English JG, et al. 2020. TRUPATH, an open-source biosensor platform for interrogating the GPCR transducerome. *Nature Chemical Biology*, **16**(8): 841–849.

Peterson LW, Artis D. 2014. Intestinal epithelial cells: regulators of barrier function and immune homeostasis. *Nature Reviews Immunology*, **14**(3): 141–153.

Polyak S, Mach A, Porvasnik S, et al. 2012. Identification of adeno-associated viral vectors suitable for intestinal gene delivery and modulation of experimental colitis. *American Journal of Physiology-Gastrointestinal and Liver Physiology*, **302**(3): G296–G308.

Reyes-Alcaraz A, Lee YN, Son GH, et al. 2016. Development of spexin-based human galanin receptor type II-specific agonists with increased stability in serum and anxiolytic effect in mice. *Scientific Reports*, **6**(1): 21453.

Reyes-Alcaraz A, Lee YN, Yun S, et al. 2018. Conformational signatures in β-arrestin2 reveal natural biased agonism at a G-protein-coupled receptor. *Communications Biology*, **1**(1): 128.

Rodrigues DJ, McLoughlin D. 2009. Using reporter gene technologies to detect changes in cAMP as a result of GPCR activation. *Methods in Molecular Biology*, **552**: 319–328.

Rogler G, Singh A, Kavanaugh A, et al. 2021. Extraintestinal manifestations of inflammatory bowel disease: current concepts, treatment, and implications for disease management. *Gastroenterology*, **161**(4): 1118–1132.

Sharma D, Malik A, Steury MD, et al. 2015. Protective role of β-arrestin2 in colitis through modulation of T-cell activation. *Inflammatory Bowel Diseases*, **21**(12): 2766–2777.

Sollenberg UE, Lundström L, Bartfai T, et al. 2006. M871—a novel peptide antagonist selectively recognizing the galanin receptor type 2. *International Journal of Peptide Research and Therapeutics*, **12**(2): 115–119.

Stearns SC, Ebert D. 2001. Evolution in health and disease: work in progress. *The Quarterly Review of Biology*, **76**(4): 417–432.

Swanson CJ, Blackburn TP, Zhang XX, et al. 2005. Anxiolytic- and

antidepressant-like profiles of the galanin-3 receptor (Gal_3) antagonists SNAP 37889 and SNAP 398299. *Proceedings of the National Academy of Sciences of the United States of America*, **102**(48): 17489–17494.

Talero E, Sánchez-Fidalgo S, Ramón Calvo J, et al. 2006. Galanin in the trinitrobenzene sulfonic acid rat model of experimental colitis. *International Immunopharmacology*, **6**(9): 1404–1412.

Tamer SA, Köse F, Yanar S, et al. 2025. Anti-inflammatory effects of spexin on acetic acid-induced colitis in rats via modulating the NF-κB/NLRP3 inflammasome pathway. *Journal of Biochemical and Molecular Toxicology*, **39**(5): e70285.

Tran A, He WY, Chen JTC, et al. 2022. Spexin: its role, regulation, and therapeutic potential in the hypothalamus. *Pharmacology & Therapeutics*, **233**: 108033.

Vanhove W, Peeters PM, Staelens D, et al. 2015. Strong upregulation of AIM2 and IFI16 inflammasomes in the mucosa of patients with active inflammatory bowel disease. *Inflammatory Bowel Diseases*, **21**(11): 2673–2682.

Violin JD, Crombie AL, Soergel DG, et al. 2014. Biased ligands at G-protein-coupled receptors: promise and progress. *Trends in Pharmacological Sciences*, **35**(7): 308–316.

Wang XJ, Xu T, Liu R, et al. 2022. High-fiber diet or combined with acarbose alleviates heterogeneous phenotypes of polycystic ovary syndrome by regulating gut microbiota. *Frontiers in Endocrinology*, **12**: 806331.

Watanabe N, Mashima H, Miura K, et al. 2016. Requirement of $G\alpha_q/G\alpha_{11}$ signaling in the preservation of mouse intestinal epithelial homeostasis. *Cellular and Molecular Gastroenterology and Hepatology*, **2**(6): 767–782. e6.

Whalen EJ, Rajagopal S, Lefkowitz RJ. 2011. Therapeutic potential of β-arrestin- and G protein-biased agonists. *Trends in Molecular Medicine*, **17**(3): 126–139.

Williams GC, Nesse RM. 1991. The dawn of Darwinian medicine. *The Quarterly Review of Biology*, **66**(1): 1–22.

Wirtz S, Popp V, Kindermann M, et al. 2017. Chemically induced mouse models of acute and chronic intestinal inflammation. *Nature Protocols*, **12**(7): 1295–1309.

Wong MKH, He ML, Sze KH, et al. 2021. Mouse spexin: (I) NMR solution structure, docking models for receptor binding, and histological expression at tissue level. *Frontiers in Endocrinology*, **12**: 681646.

Wootten D, Christopoulos A, Marti-Solano M, et al. 2018. Mechanisms of signalling and biased agonism in G protein-coupled receptors. *Nature Reviews Molecular Cell Biology*, **19**(10): 638–653.

Yeung TM, Chia LA, Kosinski CM, et al. 2011. Regulation of self-renewal and differentiation by the intestinal stem cell niche. *Cellular and Molecular Life Sciences*, **68**(15): 2513–2523.

Yu M, Wang MY, Han SY, et al. 2022. Spexin ameliorates skeletal muscle insulin resistance through activation of GAL2 receptor. *European Journal of Pharmacology*, **917**: 174731.

Zeng LX, Tao J, Liu HL, et al. 2015. β-Arrestin2 encourages inflammation-induced epithelial apoptosis through ER stress/PUMA in colitis. *Mucosal Immunology*, **8**(3): 683–695.

Zhao C, Wang HL, Liu Y, et al. 2023. Biased allosteric activation of ketone body receptor HCAR2 suppresses inflammation. *Molecular Cell*, **83**(17): 3171–3187. e7.

Zhao TT, Ye ZF, Liu Y, et al. 2022. Mutation of *spexin2* promotes feeding, somatic growth, adiposity, and insulin resistance in zebrafish. *American Journal of Physiology-Regulatory, Integrative and Comparative Physiology*, **322**(5): R454–R465.

Zheng XY, Lv YF, Li S, et al. 2017. Recombinant adeno-associated virus carrying thymosin β_4 suppresses experimental colitis in mice. *World Journal of Gastroenterology*, **23**(2): 242–255.

Zhou W, Zhang H, Huang LH, et al. 2023. Disulfiram with Cu^{2+} alleviates dextran sulfate sodium-induced ulcerative colitis in mice. *Theranostics*, **13**(9): 2879–2895.